University of Stavanger

Faculty of Science and Technology

MASTER'S THESIS

Study program/ Specialization: Petroleum Engineering, Reservoir Technology	Spring semester, 2012 Open / Restricted access
Writer: Martin Eriksen, 959225	…… (Writer's signature)
Faculty supervisor: Karl Audun Lehne External supervisor: Torunn Hana Løken, Talisman Energy Norge	
Titel of thesis: Impact of new petrophysical model to the western flank of Gyda field - understanding of reservoir quality	
Credits (ECTS):	
Key words: Petrophysics	Pages: 68 + enclosure: None Stavanger, 06.2012

Abstract

A new petrophysical model on the Gyda field has been developed during 2011 and 2012 by Ian Reid of Petro CTS. This thesis studied the performance of this on three well, and compared it to the old interpretation of the same wells. The comparison was done by comparing porosity, permeability and water saturation. The new model make use of active porosity, the fraction of pore space contributing to production, to determine permeability and water saturation from capillary pressure. The study shows that this gives a good representation of the reservoir interval, as long as the zonation is correct. The saturation height model also gives correct values as long as the Free Water Level is set to the correct height. The model does not give accurate saturation values close to the set Free Water Level.

The comparison showed very similar results between the old and new model, deviation was small and went either way.

Contents

Nomenclature

a = tortuosity factor
A = Crosselctional Area
C = Correction Factor
dL = Length Interval
dP = Pressure Difference
G = Geometrical Shape Factor
GOR = Gas Oil Ratio
GR_{log} = Gamma Ray Log readout
GR_{max} = maximun Gamma Ray log value
GR_{min} = minimum Gamma Ray log value
$haFWL$ = height above Free Water Level
$HCPV$ = Hydro Carbon Pore Volume
EOR = Enhanced Oil Recovery
ESP = Electric Submersible Pump
F = Formation Resistivity Factor
FWL = Free Water Level
k = Permeability
k_{amb} = Permeability at Ambient conditions
k_{res} = Permeability at Reservoir conditions

m = cementation exponent
$mBRT$ = meters Below Rotary Table
mMD = meters Measured Depth
$mTVDSS$ = meters True Vertical Depth Sub Sea
n = saturation exponent
N/G = Net to Gross
NGL = Natural Gas Liquids
OWC = Oil Water Contact
P_c = Capillary Pressure
P_{cAX} = Capillary Pressure in Air Brine/Mercury System
P_{cOB} = Capillary Pressure in Oil Brine System
P_{cow} = Capillary Pressure in Oil Water System
P_o = Pressure of Oil Phase
P_w = Pressure of Water Phase
P_D = Displacement Pressure
ppm = Parts Per Million
q = Volumetric Flowrate
r = Pore Throat Radius
R_t = Formation Resistivity
R_w = Water Resistivity
S_g = Gas Saturation
S_o = Oil Saturation
S_w = Water Saturation
S_{or} = Residual Oil Saturation
S_{wcap} = Water Saturation from capillary pressure
S_{wr} = Residual Water Saturation
S_{wirr} = Irreducible Water Saturation
V_{op} = Producible Oil Volume
V_{sh} = Shale Volume/Fraction, Clay Fraction/Voulme
Δt = Transit Time, Density log
Δt_f = Fluid Transit Time
Δt_{ma} = Matrix Transit Time

$\Delta\rho$ = Density Difference
θ = Contact Angle
μ = Viscosity
ν = Apparent Fluid Velocity
ρ_{fl} = Fluid Density
ρ_{fw} = Formation Water Density
ρ_{log} = Density Log readout
ρ_{ma} = Matrix Density
σ = Surface Tension, Interfacial Tension
ϕ = Porosity
ϕ_a = Active Porosity
ϕ_{amb} = Porosity at Ambient conditions
ϕ_D = Porosity from Density log
ϕ_{dt} = Porosity from Sonic log
ϕ_e = Effective Porosity
ϕ_N = Porosity from Neutron log
ϕ_{res} = Porosity at Reservoir conditions
ϕ_{tot} = Total Porosity

Acknowledgements

Acknowledgements to Torunn Hana Løken, my external supervisor, for providing an interesting topic for my thesis on behalf of Talisman Energy Norge AS, and for good guidance and help throughout this project.

Acknowledgements to Karl Audun Lehne, my faculty supervisor, for clear and direct guidance during the whole process of writing this thesis.

Further I would like to thank Sven Gundersen and Erik Rauge Andersen, petrophysicists in Talisman, both have shown no hesitation in helping me whenever needed.

- Martin

Chapter 1

Introduction

The Gyda field has produced oil and gas since 1990. First water break trough occurred July 1992 and water injection started late 2000[1]. Gyda is now approaching it's tale stage and to utilise all of the resources present, a thorough understanding of the field is essential. As a part of this elevation of understanding, a new petrophysical model has been developed.

A petrophysical model for a field gives a work flow to process and interpret log and core data, as the data are acquired through new wells. The model aims to give an accurate and correct description of the formation, still general enough to be used on several wells. The model is built on the data available at the time. As new wells are drilled, new data are obtained, the data, log and core data, is implemented and processed with the present model. When many new wells have been drilled and a lot of new data has been collected, the whole field can be evaluated over again, building a new model. This new model will be a more valid representation of the field, as more data is taken into consideration.

The scope of this study is to utilise this new petrophysical model on three wells on Gyda, see how the new model perform, and compare the results with the old interpretation of the same wells. Comparing parameters is set to be porosity, permeability and saturation. The wells that will be reviewed are 2/1-A-12, 2/1-A-32 and 2/1-A-32.

Chapter 2

The Gyda Field

The Gyda Field is situated in block 2/1 under exploration license PL 019B. The Gyda platform stands on 66 meter water depth between the Ula and the Ekofisk field, location shown in Figure 2.1. With estimated reserves of 35.90 mill Sm^3 oil, 6.30 mill Sm^3 gas and 1.90 mill tonn of NGL[2], Gyda covers an area of 57.2 km^2 and is divided into six different areas, as shown in Figure 2.2:

- C-Sand
- Downdip
- Crest
- Gyda South-west
- JU6
- Gyda South

The reservoir depth is 3700 - 4165 mTVDSS in late Jurassic Ula sandstone. Original pressure was 552 bar, which was a overpressure of approximately 140 bar. Field permeability varies within 0.5 - 1000 mD, with an average of 30 mD and porosity being approximately 16 - 20 %. Gyda South having poorer reservoir quality and different oil properties than the rest of the field. The oil at Gyda South has a gravity of 42°API with a GOR of 3500 $^{scf}/_{stb}$, whilst the rest of the field contains asphaltene-rich 40°API oil with a GOR of 1100 $^{scf}/_{stb}$[1].

There has been drilled 55 development wellbores on Gyda, where 12 production wells and 7 injection wells are active today. Oil production rate is ∼5000 $^{bblO}/_{d}$ and water production rate is ∼25245 $^{bblW}/_{d}$. Water is being

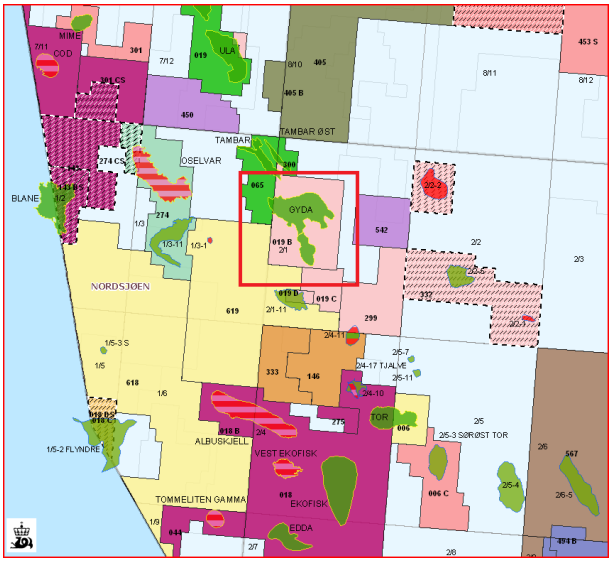

Figure 2.1: Section showing the location of the Gyda field, inside red square [3].

injected as pressure support with a rate of 34000 $^{\text{bbl}}\text{W}/\text{d}$. Electric submersible pumps (ESP) has been installed on some wells to artificially lift the well stream.

2.1 History

After the big discovery of the Groningen Field off the coast of The Netherlands in 1959, further north in the north sea was believed to be hydrocarbon bearing. Drilling started on Norwegian sector and Ekofisk was discovered Christmas 1969[5]. This discovery lead to further investigation in the area. After the Ula Field was discovered in block 7/12, a group led by BP applied for license PL 019B. The license consisted of the north west corner of block 2/1, and was awarded to the applicant group in 1977.

The first well drilled in the new license, 2/1-2, was dry. The second well, 2/1-3, struck oil in the Gyda Sandstone member of the Farsund Formation in November 1979. The Gyda Field was discovered. Well 2/1-3 was drilled to a total depth of 4297 mBRT with a pay zone in the Ula formation of 50 m, below 3819 mBRT. The well produced oil without any evidence of oil-water contact or gas-oil contact[6].

From 1982 through 1991 five appraisal wells were drilled at various locations to locate the OWC and borders of the field. In 1990 the field came on

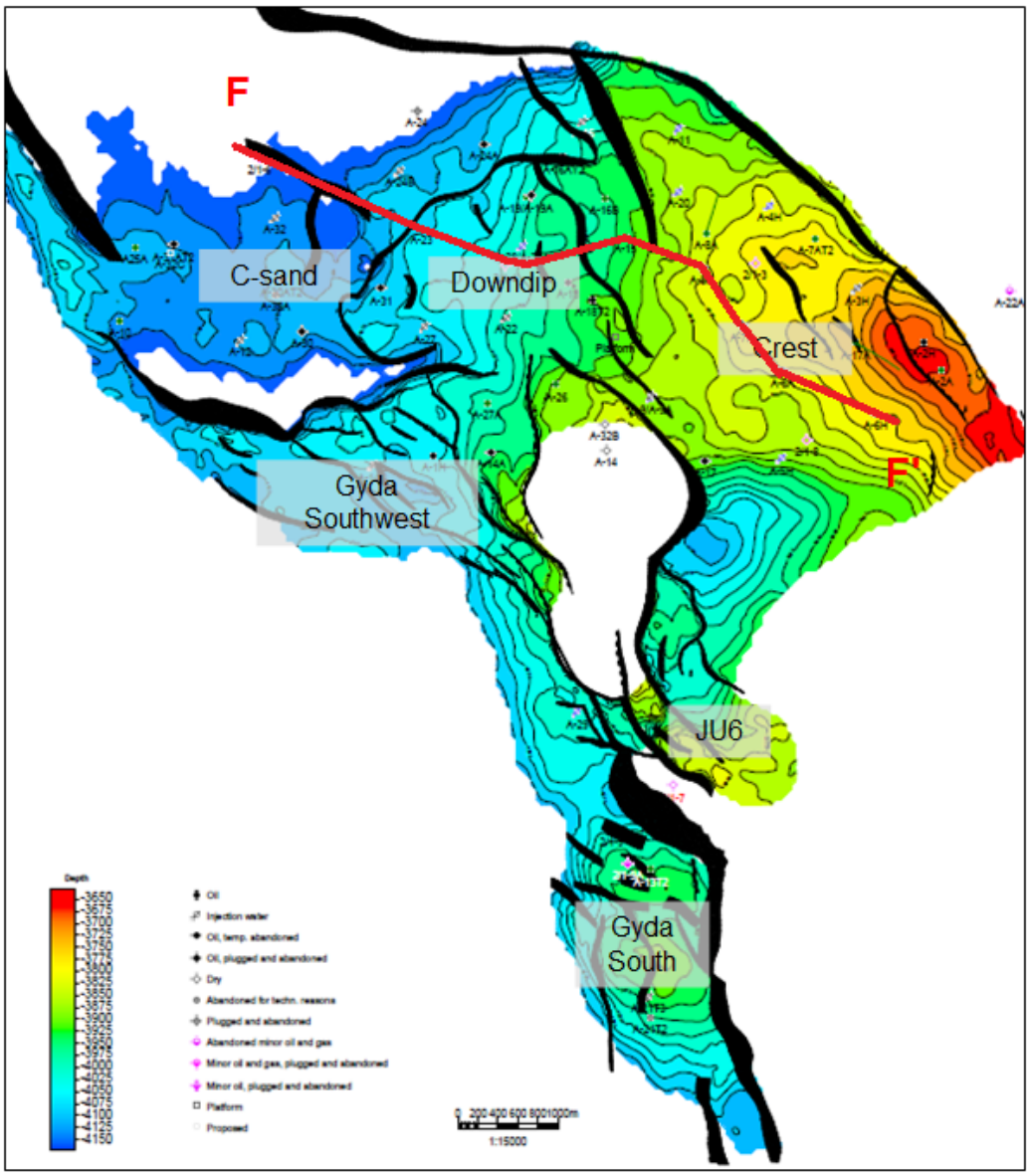

Figure 2.2: Map showing the division of the Gyda Field. See Figure 2.4 for cross section F - F'[4].

stream and began to produce. On start up Gyda was the deepest and the hottest oil field in the North Sea, with a temperature of 150°C[4].

2.2 Geology

On a basin scale, the Gyda Field is set on the Cod Terrace at the eastern margin of the central North Sea Central Graben. The Central Graben evolved during late Jurassic and early Cretaceous rifting, followed by rapid burial throughout large portions of the Cenozoic era. After a period of erosion, late Jurassic sandstones was deposited on a flat landscape. Rifting followed, leading to local compartmentalization in horsts, ridges and grabens. After this rifting period ended, late Oxfordian to early Kimmeridgian, the relative sea level rose and marine sandstones were deposited. Sandstones such as the Ula Formation, including the Gyda reservoir. Subsequently the Mandal Formation's, and the Kimmeridge Farsund Formation, organic rich mudstones were deposited in deep-marine environment forming oil prone source rock and seal for the Ula Formation[1].

The Ula Formation has its name from the Ula Field in block 7/12, and its position on the stratigraphic column is shown in Figure 2.3. The Ula Formation is extended to a wider geographic and stratigraphic range than the Ula Field itself and is sometimes called the Ula Trend. The formation stretches from the Ula Field down south-east through Tambar and to the Gyda Field. Thickness varies from 152 m in north-west to 30.5 m in the south-east. The formation is of Jurassic age, Oxfordian to Kimmeridgian.

Ula sands are generally deposited in shallow marine environment, although the deposition system varies across the formation. The formation consists generally of fine to medium grained sandstone. In the base of the formation a thin, dark grey siltstone is present. Sorting and angularity varies within the formation, depending on the deposition of the actual area. The sandstones are typically bioturbated. Downwards the Ula Formation borders on the Bryne Formation, whilst the Mandal Formation is the sealing boundary upwards. The transition border is evident when marine sandstones of Ula goes to the non marine Bryne Formation[7].

The Gyda Field is divided into three main regions, based on PVT data and structure, main field, Gyda Southwest and Gyda South. The main field comprises the Crest, Downdip and C-sand. The whole main field area lies on the hanging wall of a large fault, the Hidra Fault, which also closes the field to the north and north-east. The area plunges down east to C-sand where the reservoir is dip closed with 4-8° to the west and southwest. To the south and south-east the main field area is closed by pinch-out. Figure 2.4

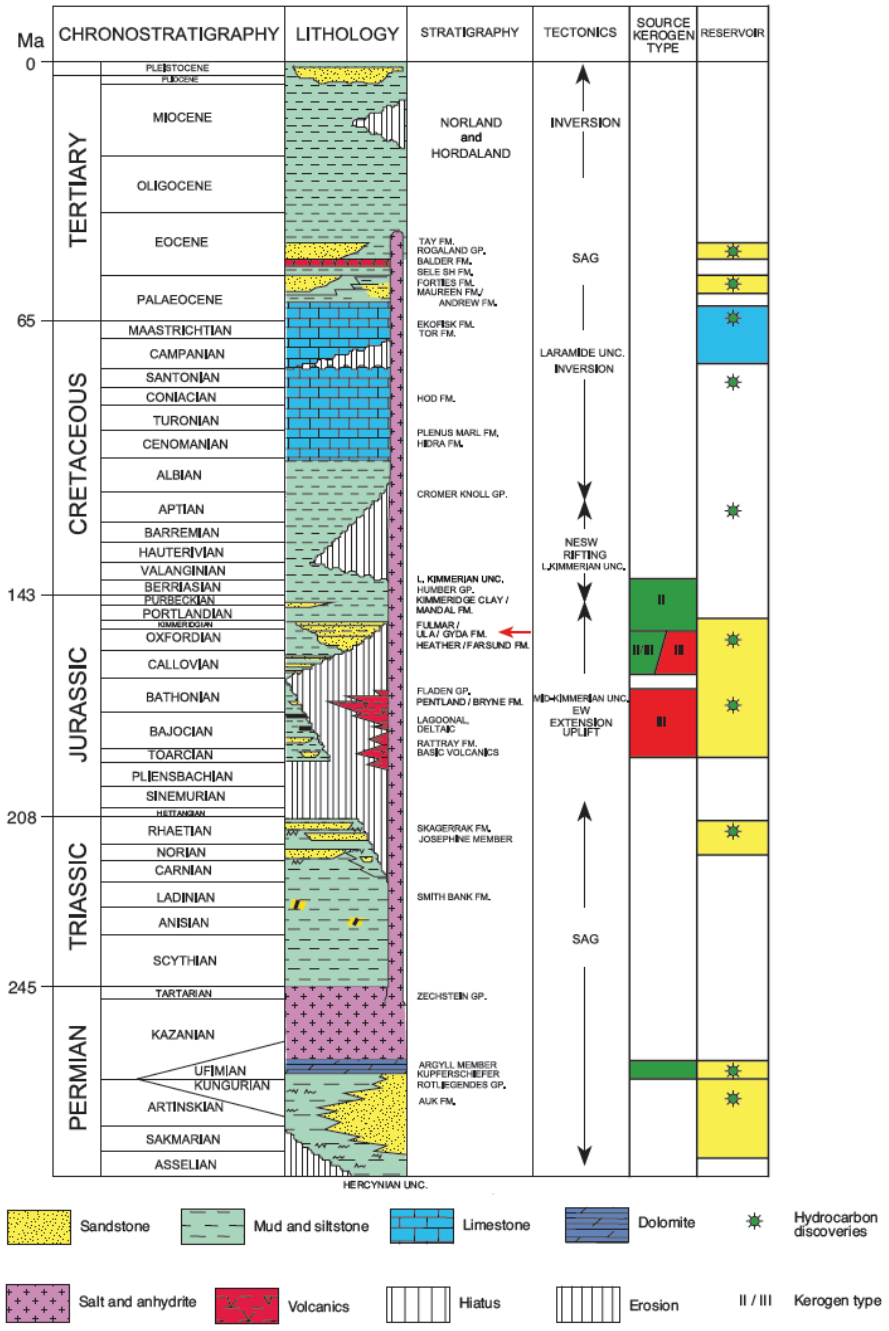

Figure 2.3: Stratigraphic column of the Central North Sea. Displaying main tectonic events, source rocks and reservoir. Red arrow indicating the Gyda producing interval[1].

displays a schematic cross section of the main field. Gyda South sits in the hanging wall to the Gyda Fault. It is a narrow and elongated structure, 1 km by 6 km, and is connected to the main field by the highly faulted Gyda Southwest.

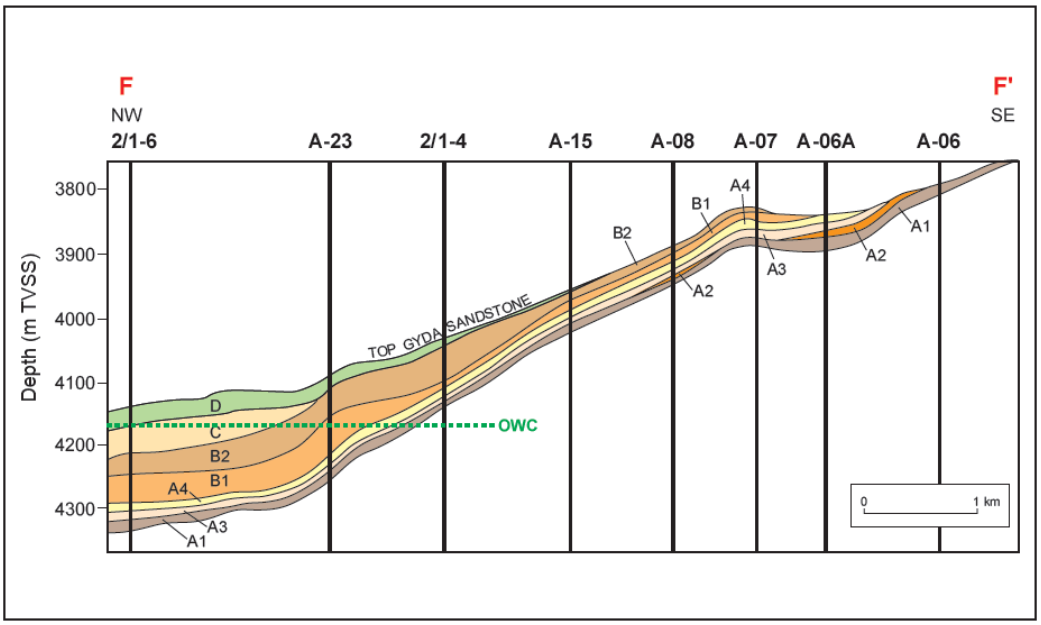

Figure 2.4: Schematic cross section of Gyda main field, F - F' sown in Figure 2.2, with dip-closure downslope and pinch-out up at crest[1].

The hydrocarbon bearing layer at the Gyda Field is the "mid-late" Kimmeridgian sandstone, which falls on the Ula Trend. The Gyda sandstone lies with the marine shales of the Kimmeridgian - Volgian Farsund Formation both above and below, except in minor areas where the Haugesund Formation lies below. The stratigraphical pinch-out is caused by Zechstein salt movement along the Cod Terrace. The sandstones of the Ula trend was deposited in a shallow marine shelf-environment. Storm dominated periods deposition with rapid cementation were followed by periods of quiet water and heavy bioturbation. The sandstones are both fining and coarsening upwards, reflecting changes in sediment supply, subsidence and/or sea level change.

The Gyda sandstone member is divided into four main depositional units, A to D, where A is deepest and oldest and unit D is non reservoir. As shown in Figure 2.4. The reservoir units are further subdivided into nine sequences, reservoir zone 1 to 9. Unit C consists of sub zones 1 - 3, unit B sub zones 4 - 6 and unit A with sub zones 7 - 9. This division is based on the characteristics

of each zone and different values of parameters is assigned each zone in the calculation of hydrocarbon content. Unit A is a prograding unit, whereas unit B and C were deposited under a period of reduced deposition and is aggradational. Unit D is a retrograding unit where the sea level rose. All units thins towards the crest, unit C, the C-sand is only present down dip as consistent with the earlier areally zonation. Erosion of units A and B at crest is believed to be source for units C and D, along with minor contributions from sediment sources far off[1].

Chapter 3

Petrophysical Parameters

The major purpose of a petrophysical study is to determine if, and how much, hydrocarbons are present in the drilled formation. This is done by looking at logs, determining several properties for the formation. Below there is a general review of these properties, before the special interpretation for the Gyda field is presented.

Hydrocarbon pore volume (HCPV) is the measurement of how much of hydrocarbons are present in the reservoir. This is calculated using following formula

$$\text{HCPV} = \text{gross rock volume} \cdot \phi \cdot (1 - S_{wr} - S_{or}), \tag{3.1}$$

where *gross rock volume* is the entire reservoir volume, that is the area of the field times the height of the reservoir column. Rest of the parameters in equation (3.1), ϕ, S_{wr} and S_{or} are explained and derived below.

3.1 Porosity

The porosity of a rock , ϕ, measures the capacity a rock has to hold fluid in between the matrix grains. Porosity can be quantitatively determined through the ratio

$$\phi = \frac{\text{pore volume}}{\text{bulk volume}}, \tag{3.2}$$

where *pore volume* denotes the interstitial volume and *bulk volume* denotes the total rock volume. From this it is evident that porosity is a fraction between zero and one and is often given in percent. Figure 3.1 shows the rock matrix and the interstitial fluid. Note that the figure is illustrative, in real life porosity seldom exceeds 30 %.

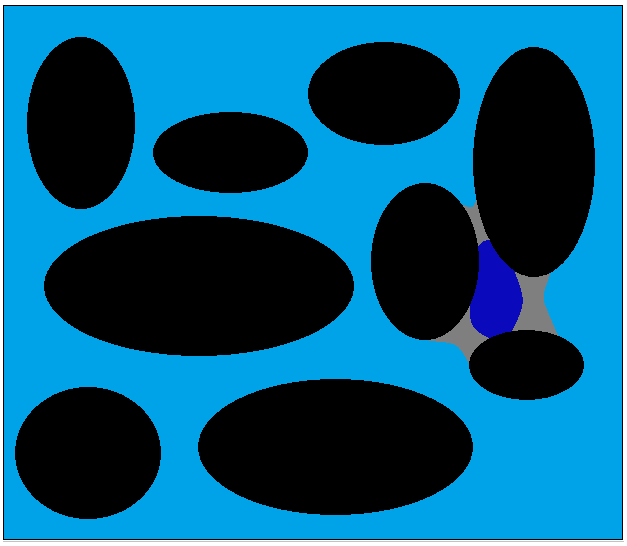

Figure 3.1: Schematic figure showing porosity as the blue void in between the black rock matrix. Isolated pore showed containing trapped fluid (deeper blue).

Some of these pores can be isolated from the rest of the pores due to cementation and compaction during the formation of the rock. These isolated pores do not contribute to the volume of fluid that can be produced, e.g oil. Following this, the porosity is subdivided into two categories:

- Total porosity
- Effective porosity

The total porosity, ϕ_{tot}, follows equation (3.2) but can further derived to

$$\phi_{tot} = \frac{\text{total pore volume}}{\text{bulk volume}}, \tag{3.3}$$

$$\phi_{tot} = \frac{\text{bulk volume} - \text{grain volume}}{\text{bulk volume}}. \tag{3.4}$$

The effective porosity, ϕ_e, is given by

$$\phi_e = \frac{\text{interconnected pore volume}}{\text{bulk volume}}, \tag{3.5}$$

where *interconnected pore volume* is the pore volume that is connected and thus producible[8].

3.2 Clay and Porosity

Clay minerals are not only present in shale formations, they are also appearing in clastic hydrocarbon reservoirs like sands or chalks. In fact, clean sand or chalks formations are rather the exception than the rule. Consequently the shale volume, V_{sh}, is defined as the amount of shale\clay present in a formation. This is a fraction where V_{sh}=0 is a clean sand, and V_{sh}=1 indicates clean shale. Shale influences the porosity of the reservoir and can be distributed in three different manners, also shown in Figure 3.2, dispersed, laminated and structurally:

Dispersed shale or dispersed clay minerals are formed from precipitation of pore fluid following chemical-, pressure-, or temperature-changes during the formation of the reservoir rock, called diagenetic formation. Clay is formed as an integrated structure on the pore walls. These can grow together through pore throats and form complex structures. Dispersed clay strongly influences the porosity and permeability of the reservoir.

Laminated shale are formed outside the framework of the reservoir rock, they are of so-called detrital origin. These thin layers of shale does not influence the porosity or permeability of the reservoir rock. They do however form tight barriers vertically, and serve as horizontal permeability barriers.

Structural clay is also formed diagenetic, where small pellets of clay is deposited simultaneously with the clastic reservoir sediments. This has small or no effect on the performance of the reservoir rock[9, 10].

Stated above, the dispersed clay influences the porosity to a large extent. The clay does not only block pore throats and isolate pore fluid, clay also bind water, increasing the water saturation making it irreducible water. This water is bound from two different, but closely related phenomena. The clay crystals, mainly stacked silicate layers, become negatively charged when they contact water and binds water to the surface of the crystal, called adsorbed water. The ions that are expelled during the "charging" of the crystals do also attract water molecules, this water is called hydrated water. The adsorbed water plus the hydrated water form the bound water, see Figure 3.3[9, 10].

Taking the bound water into consideration the porosities can be defined over again. The total porosity consists of the volume of hydrocarbons, free water and the volume of bound water. The effective porosity is on the other hand only the volume of hydrocarbons and free water. This is shown schematic in Figure 3.4.

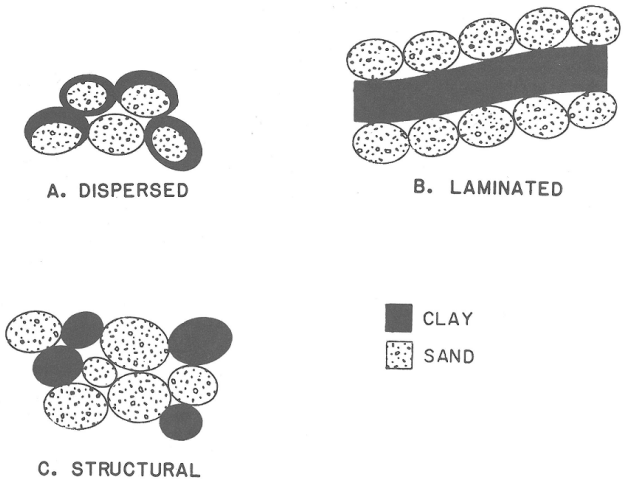

Figure 3.2: Illustration of ways that shale can be distributed in porous rock[9].

3.3 Saturation

The pore space in a reservoir rock is filled with fluid. The amount of fluid in the pore space gives the saturation through the ratio

$$\text{fluid saturation} = \frac{\text{total volume of fluid}}{\text{pore volume}}, \tag{3.6}$$

from this it is evident that saturation is a fraction between zero and one which also can be given in percent. The fluid occupying the pore volume is usually oil, water, gas or several of them at once. If a porous rock contains water only, the given rock is 100 % water saturated. Formula for all three saturations are

$$S_{o,w,g} = \frac{V_{o,w,g}}{\text{pore volume}}, \tag{3.7}$$

where S is the saturation, V is the volume of fluid and *o, w, g* denotes oil, water and gas respectively. The pore space must be totally filled with fluid, which yields the relation

$$S_o + S_w + S_g = 1. \tag{3.8}$$

For these fluids the residual saturation can be introduced. This saturation is the lowest saturation obtainable for the given fluid. In an untouched, oil

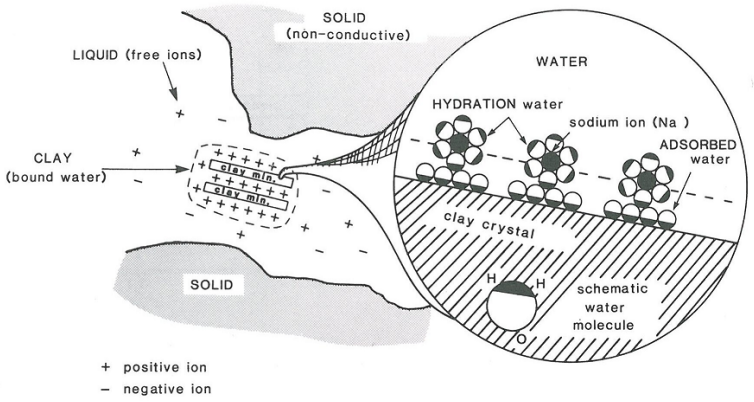

Figure 3.3: Illustration of clay bound water. Section displays the adsorbed and hydrated water[11].

filled reservoir, there are always a small amount of water present. This water is "clinging" to the rock surface and has not been replaced by the oil when the oil migrated to the reservoir. This amount of water is the residual water, giving the residual water saturation, S_{wr}. Figure 3.5 shows the situation described above. As the reservoir contains just oil and water, and the saturations always sum to one the oil saturation now becomes

$$S_o = 1 - S_{wr}. \tag{3.9}$$

As for water, there are also a residual oil saturation, S_{or}. This saturation is determined when the oil stop flowing under production of the reservoir and no more oil can be produced. Having these two saturations is important in volumetric calculations, as the expression for producible oil in the reservoir, V_{op}, becomes

$$V_{op} = 1 - S_w - S_{or}. \tag{3.10}$$

The residual saturations are a result of the wetting properties of the fluid, which are influenced by interfacial tension and capillary pressure. The residual saturation you first get is for one given process, this saturation can be lowered by secondary draining with EOR methods. However, there will always be a residue of fluid due to wetting preferences, this saturation is called the irreducible saturation. If water is the fluid in question the notation S_{wirr} is used[8, 13].

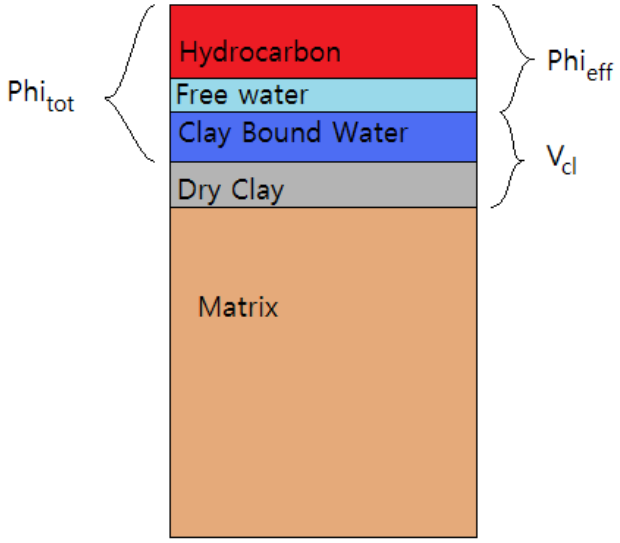

Figure 3.4: Schematic view of a reservoir segment. ϕ_{tot} being marked on the left side and ϕ_e on the right side[12].

3.3.1 Determine Water Saturation, The Archie Equation

The Archie equation determines the water saturation from well logs. The equation relates water saturation with porosity and formation resistivity, and was proposed by Gus Archie in 1942,

$$R_t = \frac{a}{\phi^m}\frac{R_w}{S_w^n}, \tag{3.11}$$

where the parameters are defined as:

$\mathbf{R}_t$ = resistivity for hydrocarbon bearing rock

$\mathbf{R}_w$ = resistivity of the formation water

ϕ = porosity

$\mathbf{S}_w$ = water saturation

$\mathbf{a}$ = tortuousness factor

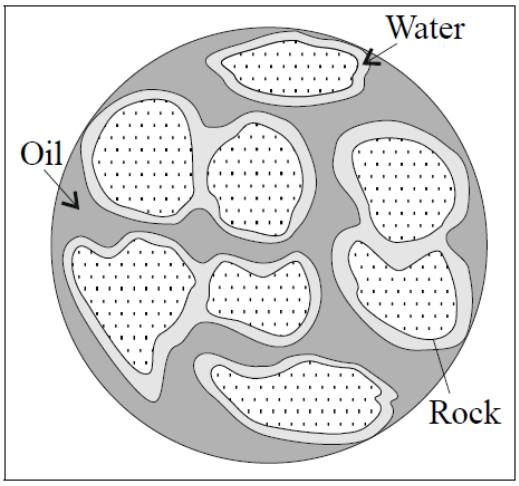

Figure 3.5: Oil and water in a water-wet porous reservoir rock. The water being the residual water[13].

m = cementation exponent

n = saturation exponent

Rearranged for water saturation, equation (3.11) becomes

$$S_w = \sqrt[n]{\frac{a\,R_w}{R_t\,\phi^m}}. \tag{3.12}$$

The parameters a and m are closely related through the formation resistivity factor, F, which is incorporated in the Archie equation

$$F = \frac{a}{\phi^m}. \tag{3.13}$$

One of the assumptions for the Archie equation is that the rock matrix itself, not is electro conductive, thus the formation water is the only conductor. This does not exclude the rock from influencing the resistivity. The influence of the rock is governed by the porosity and other factors such as pore geometry and cementation, for these last factors the formation resistivity factor is introduced. As stated above, the water is the only conductor, but the distribution of water is determined by the rock in the same way that traffic is determined by the road. If the road is narrow and winding, the traffic goes slowly with low passage. On the other hand the traffic goes with a fast and steady flow on a motorway. The F-factor is analogues to this,

where low F-factor gives good conductivity and high F-factor gives poor conductivity. Figure 3.6 exhibits different F-factors for constant porosity. The a is a measure of the tortuosity of the pore space, considering compaction, pore structure and grain size. a is in most cases set to 1. m is the cementation exponent, where an ideal pore space of parallel capillary tubes would yield a value of 1. The typical value for the m is around 2. The last new parameter in equation (3.11) is the n, the saturation exponent. This parameter is dependent on the presence of nonconductive reservoir fluid, such as hydrocarbons, and is also set to around 2.

There are some limitations for the Archie equation. The main assumption of nonconductive rock matrix is important, but not always valid. If the rock contains some clay minerals, there will be conductance through the rock itself. This can either be indirectly compensated through the formation resistivity factor, or there are other models, taking this into account, such as the Waxman-Smiths equation[11, 14, 9].

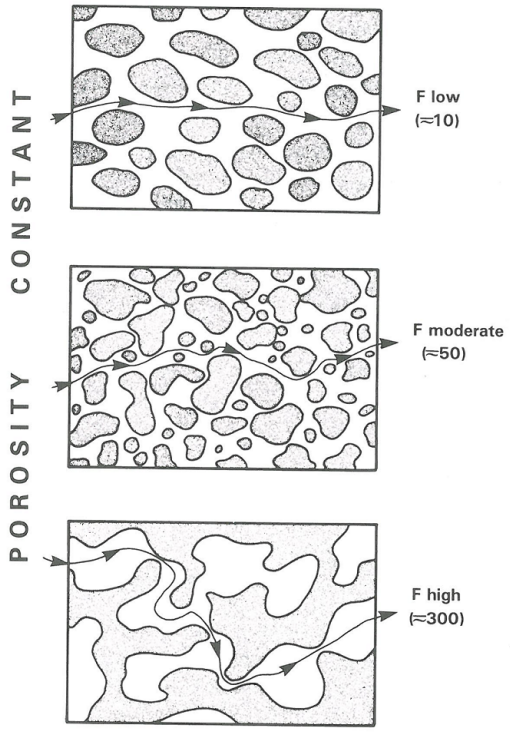

Figure 3.6: Figure showing three different formation resistivity factors. Constant porosity[11].

3.4 Wettability, Capillary pressure and Free Water Level

The properties that determines the saturation in a reservoir are mainly wettability and capillary pressure.

3.4.1 Wettability

Wettability is defined as *the tendency of one fluid to spread on or adhere to a solid surface in the presence of other, immiscible, fluids*[8]. The most significant parameter to measure the wettability is the contact angle, θ. In Figure 3.7 the contact angle for three different fluids are displayed, mercury, oil and water. The contact angle decreases with increasing wettability, where *intermediate* wettability is associated with a contact angle from 60° to 90°. Under these conditions, the liquid will usually be repelled from the surface[8].

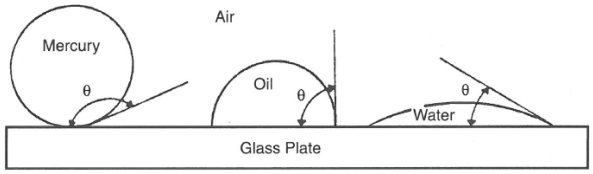

Figure 3.7: Figure showing three droplets of different fluids and contact angle[8].

3.4.2 Surface tension

Surface tension and interfacial tension, σ, are properties of a immiscible fluid which heavily influences the capillary pressure of the system. Surface tension is a tension that arises over the boundary between a liquid and a gas, whilst interfacial tension is between two liquids. The best known surface and surface tension is the one between water and air, which one sees every day on the top of a glass of water. The tension is a result of unbalanced forces at the boundary between the two fluids. A molecule situated at the boundary experiences forces from both its own molecules and the molecules of he other fluid. These forces are not balanced and the surface tension arises to balance these forces out. A schematic representation of this is shown in Figure 3.8. The SI-unit of surface tension is $^{N}/_{m}$, however $^{mN}/_{m}$ is used as it is a more appropriate order of magnitude. The cgs unit of surface tension is $^{dyn}/_{cm}$ and $1\ ^{dyn}/_{cm} = 1\ ^{mN}/_{m}$. The surface tension of water at 20°C is σ= 72.8 $^{mN}/_{m}$[15].

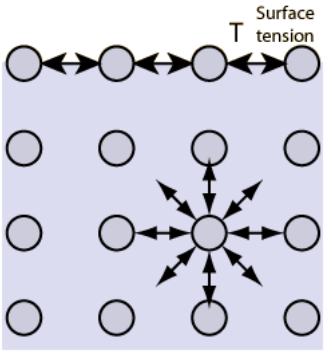

Figure 3.8: Schematic illustration of surface tension. The forces between the molecules at the fluid boundary is larger, causing surface tension[15].

3.4.3 Capillary Pressure

When two immiscible fluids are in contact there is a pressure discontinuity across the interface. The magnitude of this pressure is called the *capillary pressure*, P_c, and is dependant on the interfacial tension of the system and the curvature of the interface. The expression being

$$P_c = P_{non-wettingphase} - P_{wettingphase}. \tag{3.14}$$

The pressure excess of the capillary pressure determines the saturation of the non-wetting fluid in a porous medium. For higher capillary pressures, smaller pores are invaded by the non-wetting phase, thus increasing the saturation of the non-wetting phase. The relationship between saturation in a porous medium and the capillary pressure is shown in Figure 3.9. From the figure it is evident that fully saturated by the non-wetting phase, the system has a capillary pressure of zero. The capillary pressure increases, with the saturation unchanged until the capillary pressure called P_D is reached. This pressure is called the displacement pressure and is defined as the lowest capillary pressure needed to introduce the non-wetting phase in the largest pores present. As the capillary pressure rises further, the saturation of the non-wetting phase increases until the critical saturation of the wetting phase is reached.

To utilise this in a reservoir system, containing oil and gas, following the above notation from equation (3.14), the formula for the capillary pressure becomes

$$P_{cow} = P_o - P_w. \tag{3.15}$$

This system is shown in Figure 3.10, and introduces some new terms.

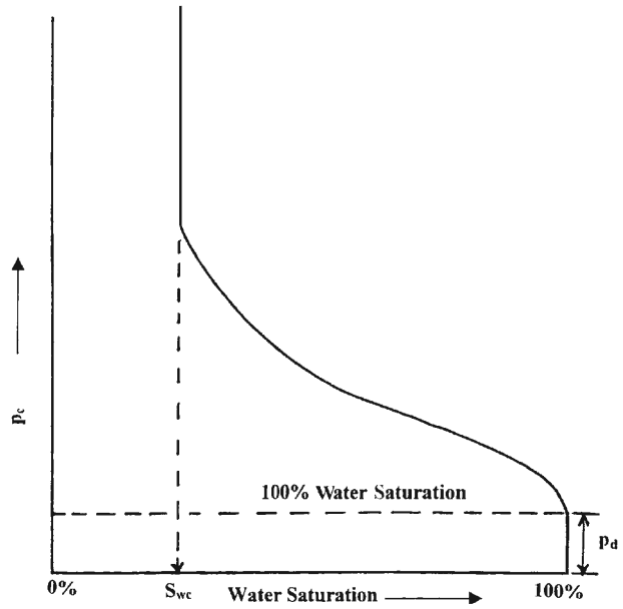

Figure 3.9: Diagram showing the relation between capillary pressure, P_c, and saturation of the wetting phase (water), S_{wc}[8].

The free water level(FWL) is any height in the reservoir where the water saturation is 1.0. On the y-axis the height over FWL is shown. The height becomes analogues to the capillary pressure, following a relation of the density differences of the fluids and interfacial tension. At the height where the water saturation begins to decrease, corresponding to P_D in Figure 3.9, the oil-water contact (OWC) is determined. From $S_w = 1$ the saturation decreases down to S_{wr}. This interval where the water saturation decreases is called the transition zone and its height is determined by the density difference of water and oil.

Production above the transition zone would be just oil, as the residual water is immobile. Production from the transition zone will be both water and oil and production from below the OWC would accordingly be water only. For a system also containing gas, the boundary region between oil and gas will be completely analogues to the water - oil case[13, 8].

3.5 Permeability

Permeability, k, is the property of the porous medium that measures the capacity and ability to transmit fluids[8]. If there are no interconnected pores

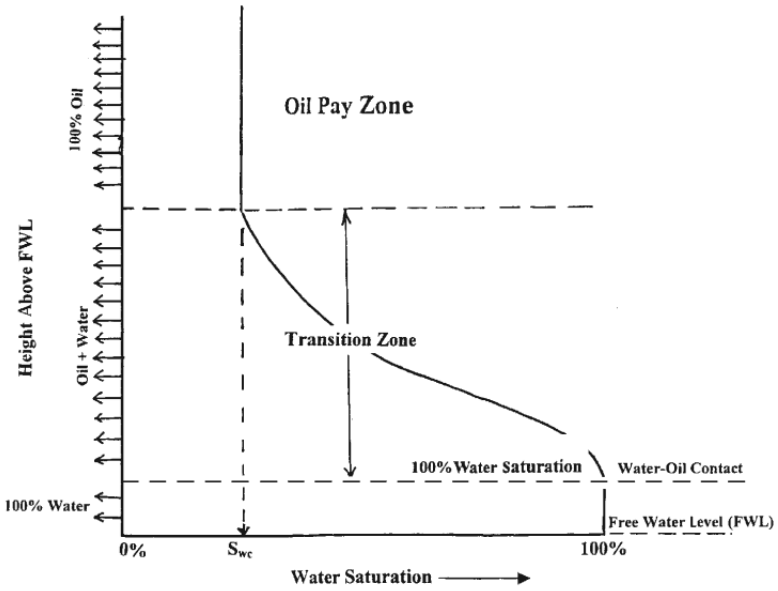

Figure 3.10: Water saturation as a function of capillary pressure, or height over free water level. Free water level, oil water contact and transition zone shown[8].

in the reservoir rock, the permeability is zero. This parameter is important for the reservoir quality as it controls the flow rate and flow direction of the fluid contained in the porous medium. The permeability is expressed through Darcy's law

$$\nu = -\frac{k}{\mu}\frac{dP}{dL}, \tag{3.16}$$

where the flow is with incompressible fluid trough a core sample with length L and area of cross-section A. ν being apparent fluid flowing velocity, $^{cm}/_{sec}$, k the proportional constant or permeability, μ the viscosity of the fluid flowing, cp and $^{dp}/_{dL}$ pressure drop per unit length, $^{atm}/_{cm}$.

Worth noting is that the velocity ν here not is the true velocity, but an apparent velocity found by dividing the flow rate by the cross sectional area. This velocity can be replaced with q/A leaving equation 3.16

$$q = -\frac{kA}{\mu}\frac{dP}{dL}, \tag{3.17}$$

where q is flow rate through the porous medium, $^{cm^3}/_{s}$ and cross sectional area in cm^2[8, 13].

3.6 Net to Gross

Once the HCPV have been calculated from equation (3.1), it is of interest to determine the amount og these that can be produced, the Net to Gross ratio, N/G, gives exactly that. It is defined as *the portion of reservoir rock which is considered to contribute to production*[16], and is a fraction between 0 and 1. The formula for recoverable resources then becomes

$$\text{Recoverable Resources} = \text{HCPV} \cdot \text{N/G}, \tag{3.18}$$

with HCPV from equation (3.1).

Net to Gross is determined through a series of cut-off values. These are values determined for each reservoir parameter. The value that, for the given parameter in a given zone, yields such a negative contribution to the reservoir performance that production from said zone halts. Often the cut-off value for permeability is set to 1 mD, which means that reservoir sections having a permeability less than this is cut off from the volumetric calculation. This is done for all parameters influencing the reservoir like porosity, saturations and shale volume. Worth noting that Net to Gross is a dynamic parameter. Say the cut off for permeability is set to 1 mD for an oil bearing zone, the cut off for a gas zone could be set to 0.001 mD[16].

Chapter 4

Petrophysical Model

The new petrophysical model on Gyda Field is developed by Ian Reid, Petro CTS Ltd. This study aims to utilise this and see the impact of this new model on selected wells.

4.1 Porosity

Ian Reid's model uses a total porosity scheme. The total porosity is found from the density log, values for ρ_{fl} and ρ_{ma} along with other values are found in Table 5.3. The total porosity from log yields good correlation with overburden corrected core porosity, thus the core porosity is the total porosity.

The formula for total porosity is the standard formula,

$$\phi_D = \frac{\rho_{ma} - \rho_{log}}{\rho_{ma} - \rho_{fl}}, \tag{4.1}$$

where ρ_{ma} is the matrix density, ρ_{fl} is the fluid density and ρ_{log} is the continuous reading from the log. In absence of density log measurements, sonic log should be used with coherent formual,

$$\phi_{dt} = \frac{\Delta t - \Delta t_{ma}}{\Delta t_f - \Delta t_{ma}}, \tag{4.2}$$

where Δt_{ma} and Δt_f denotes the interval travel time of the matrix and pore fluid, respectively. Δt is the continuous reading from the log.

The overburden correction for core porosities are given by

$$\phi_{res} = 0.94 \cdot \phi_{amb}, \tag{4.3}$$

where ϕ_{amb} is the core porosity and ϕ_{res} is the corrected porosity. This correction is taken from the DONG study of 2011[17]. Here a large set of

cores have been reviewed and thorough looked at the burial stresses with respect to the porosity reduction ratio. The usual effective porosity is not derived and used in the new model, instead active porosity is defined. The low clay volume in the Gyda sandstones gives a other cause of pore fluid containment than the one shown in Figure 3.1. The active porosity is defined and explained in a below section.

4.2 Clay fraction

The calculation of the clay fraction is preferred done with the double clay indicator. This is a cross plot method, see Figure 4.1 for the actual cross plot, with ϕ_N on the x-axis and ϕ_D on the y-axis. The diagonal in the first quadrant is the clean line, plotting the two porosities representing a clean, clay-free, formation point, the point will fall on the clean line. A point in the cross plot called the shale point, which represents shale formation, is also plotted and a line drawn to origin, called OS. Isoporosity lines are drawn parallel to OS and isoshale-content lines are drawn parallel to the clean line. Any point plotted representing a clay bearing formation will fall between the clean line and OS and the porosity and clay content, ϕ and V_{sh}, is determined by the relative position to the triangle[9].

If data from neutron and/or density logs are unreliable or absent, the gamma ray should be used following the standard formula,

$$V_{sh} = \frac{GR_{log} - GR_{min}}{GR_{max} - GR_{min}}, \tag{4.4}$$

where GR_{min} is the log value for clean sand, GR_{max} is the log value for shale and GR_{log} is the continuous log reading.

4.3 Water saturation

Water saturation is calculated with the Archie equation with a, m and n values determined from core analysis. The values are collected from the DONG study of 2011[17]. Seeing that this study had a comprehensive set of relevant core data. The Archie equation rearranged for water saturation was given in equation 4.5 and looked like

$$S_w = \sqrt[n]{\frac{a\, R_w}{R_t\, \phi^m}}. \tag{4.5}$$

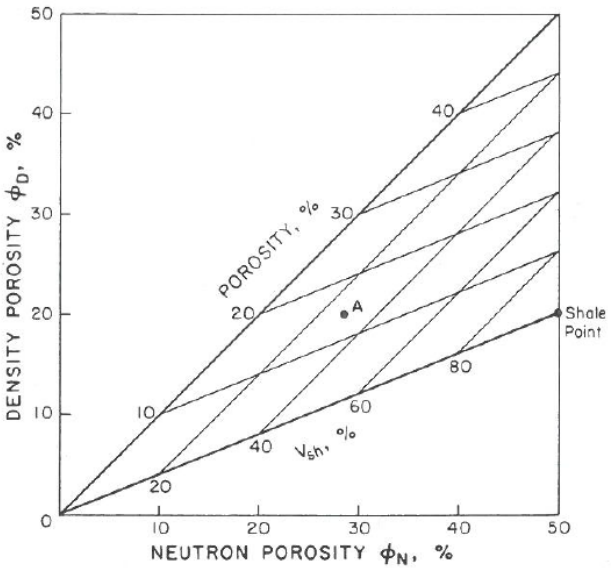

Figure 4.1: A neutron-density cross plot for clay fraction determination with the clean sand line on the diagonal, the shale point and a arbitrary point A. The formation point A represents will have V_{sh}=30% and ϕ=15. Note that the porosities are cut at 50% on the axis[9].

The constants a, m and n are set to:

$$a = 1$$
$$m = 2.08$$
$$n = 2.02$$

Furthermore the formation water resistivity, R_w, is set to 0.048 $^{ohm}/_{m}$ at 20 °C, which is equivalent to 210,000 ppm NaCl. At reference depth 4065 m TVDSS and 156 °C, R_w is set to 0.0116 $^{ohm}/_{m}$[18]. There has been different studies on Gyda, all surveys have indicated a salinity of the formation water in the range of 200 - 220 kppm, this is regarded as correct despite lack of virgin water sample. RFT plot for well 2/1-6 is shown in Figure 4.2, this plot gives a formation water density, ρ_{fw}, of 1.07 $^{g}/_{cm^3}$ which is consistent with said salinity interval.

4.4 Net to Gross

The determining factor to determine net sand is a parameter called active porosity or active pore space, ϕ_a. Active porosity is defined as the fraction of

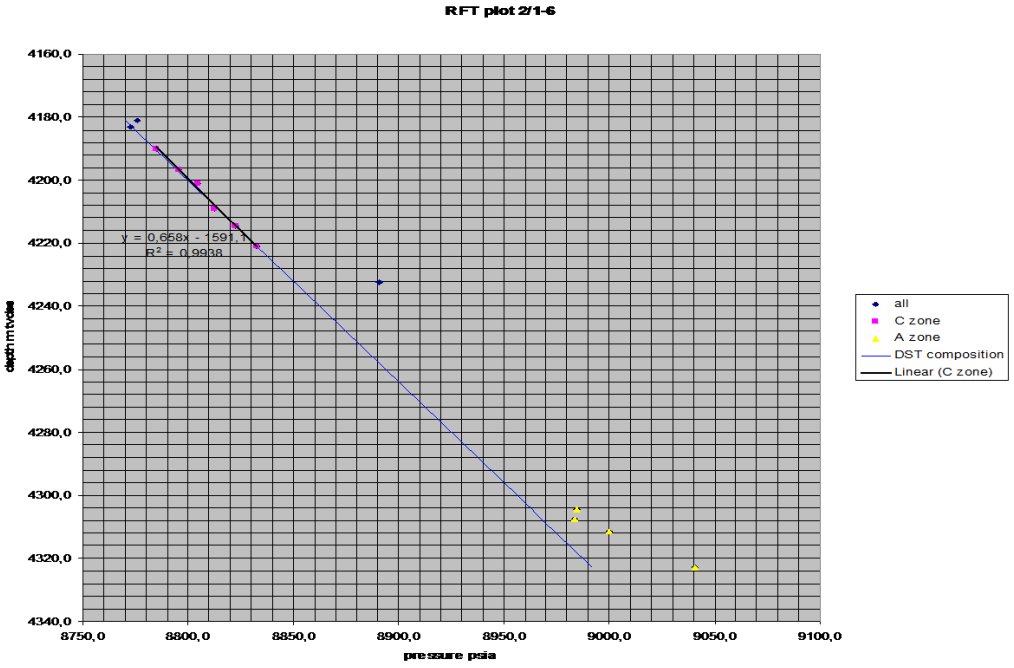

Figure 4.2: RFT-plot for well 2/1-6, pressure (Psia) plotted against depth (mTVDSS). Using linear trend, gives a formation water density of 1.07 $^{g}/_{cm^3}$[18].

the pore space that has been charged by hydrocarbons and thus contribute to production. The decisive factor in determining whether the pore space is active and passive is the pore throat radius, r, through the assumption that pore size and pore throat radius is closely connected. On basis of the pore throat radius is directly linked to the capillary pressure through

$$P_c = \frac{2\sigma cos(\theta)}{r}, \tag{4.6}$$

where σ and θ is the interfacial tension and the contact angle of the system respectively. Knowing the capillary pressures from cores, the pore throat radius distribution for the whole field can be easily made. This has been done in Figure 4.3 with the assumption of constant interfacial tension and contact angle[19]. This revealed a bi-modal distribution of the pore throat size. The evaluation of the whole field revealed the split in the distribution to be in the interval 0.5 - 1.0 μm with r = 0.6 μm chosen as average, and as the split for active and passive pore space.

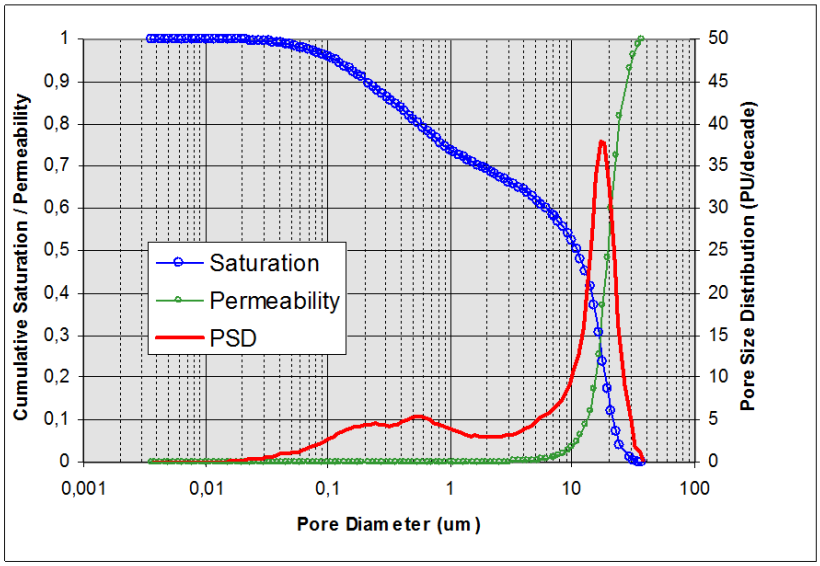

Figure 4.3: Pore diameter plotted against distribution, cumulative saturation and permeability. A pore diameter of 1.2 μm, equivalent a pore throat radius of 0.6 μm chosen as the split for active/passive pore space[18].

Once the active pore space is defined a plot of active vs total porosity can be made. This has been done in Figure 4.4, here the porosity points have been divided in reservoir units A, B and C. The plot reveals that unit B differs somewhat from unit A and C, this in mind A and C has been combined

whilst unit B is kept separate. The new datasets are re-plotted in Figure 4.5, where also trend lines are added to the two data series. Net sand is defined present if ϕ_a is greater than zero. Also from the trend lines the formula for the active porosity is given seeing that ϕ_a= f(ϕ_t).

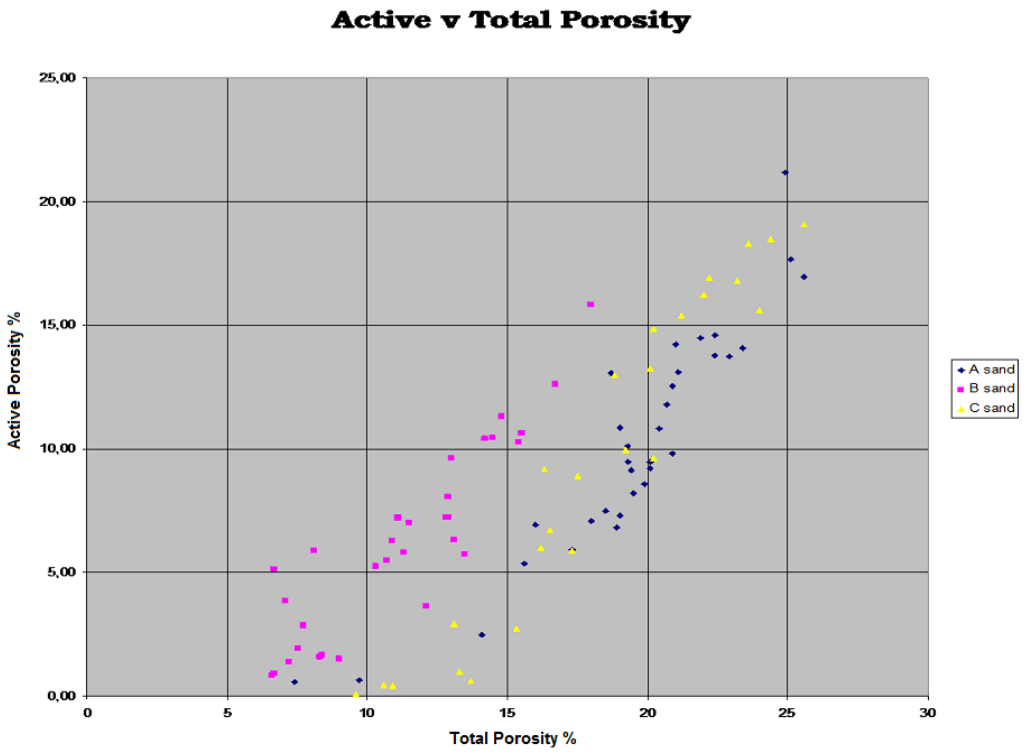

Figure 4.4: Total porosity plotted against Active Porosity for A(squares), B(diamonds) and C(triangles) unit[18].

The cut off values for the total porosity and thus net sand becomes 12.2 % for A and C units and 5.3 % in the B unit. The formulas relating ϕ_a to ϕ_t are:

For A and C units

$$\phi_a = 1.44\phi_t - 17.6, \tag{4.7}$$

for the B unit

$$\phi_a = 1.065\phi_t - 5.692, \tag{4.8}$$

where all porosities are given in percent.

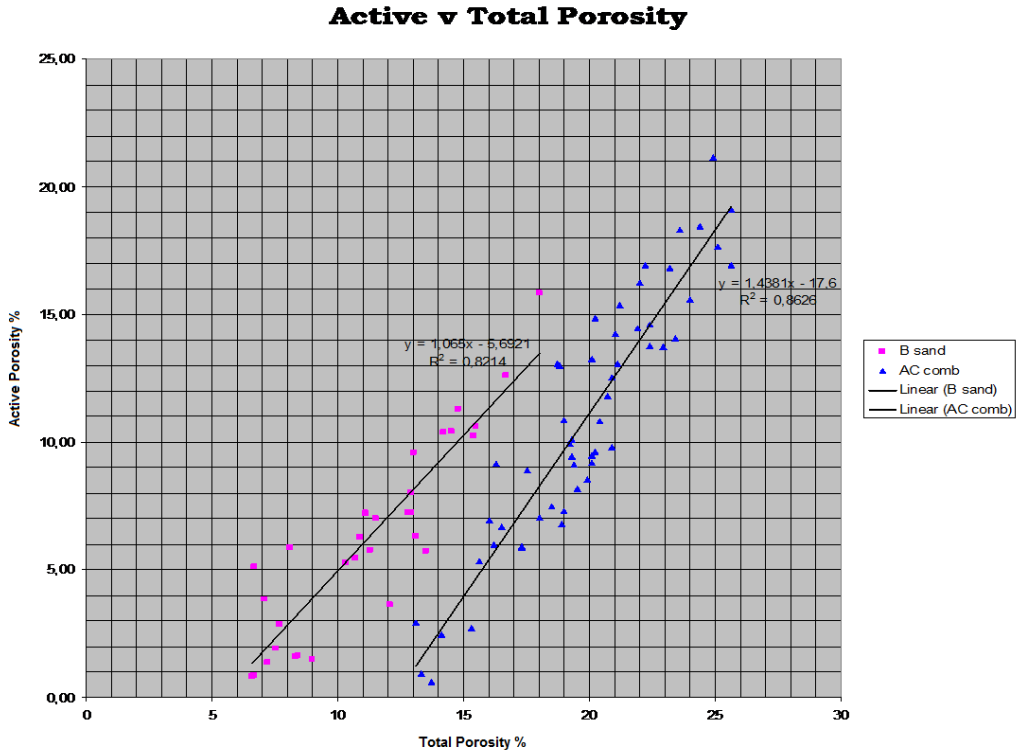

Figure 4.5: Total porosity plotted against Active Porosity for A and C units combined and B unit. Trend lines added making it possible to establish a relationship between total and active porosity[18].

4.5 Permeability

Once the active pore space is determined it is easy to show that ϕ_a gives a better correlation with permeability than ϕ_t for each reservoir unit. This is evident in Figure 4.6 and Figure 4.7, where scatter is considerably reduced when plotting "poroperm" for ϕ_a.

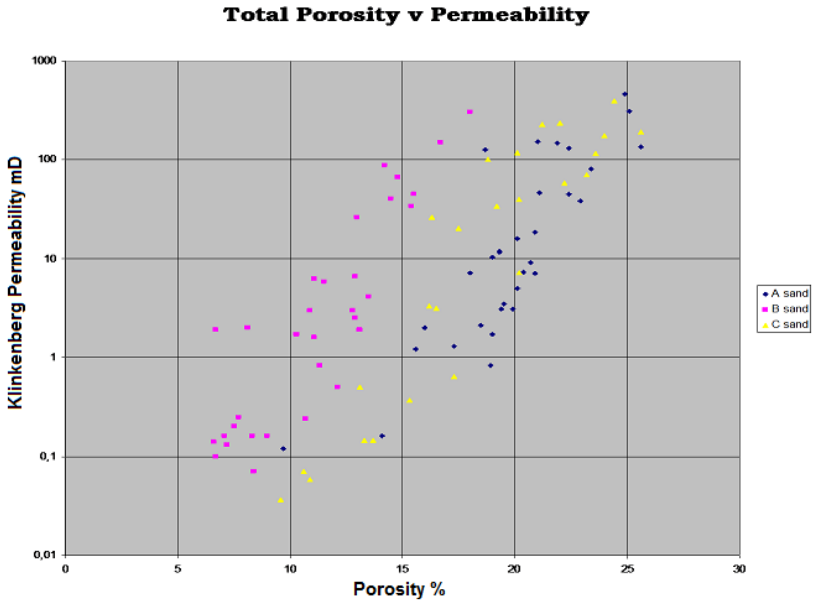

Figure 4.6: Permeability plotted against total porosity for the three reservoir units. Permeability in mD on logarithmic scale, porosity in %. Obvious trend but large scatter[18].

Furthermore we can look at Figure 4.4 in section 4.2 to justify the same lumping of zones A and C for the permeabilities as for the porosities. The resulting permeability functions trend lines are displayed in Figure 4.8 with the following formula belonging to the trend lines[18]:

For the A and C unit

$$k = 0.0005 \cdot \phi_a^{4.52}, \tag{4.9}$$

for the B unit

$$k = 0.000185 \cdot \phi_a^{5.276}, \tag{4.10}$$

where ϕ_a inserted in percent.

To correct the permeabilities from lab, k_{amb} to reservoir conditions, k_{res} following formula is taken from the 1993 BP model[20]

$$k_{res} = 0.719 \cdot k_{amb}^{0.9958}. \tag{4.11}$$

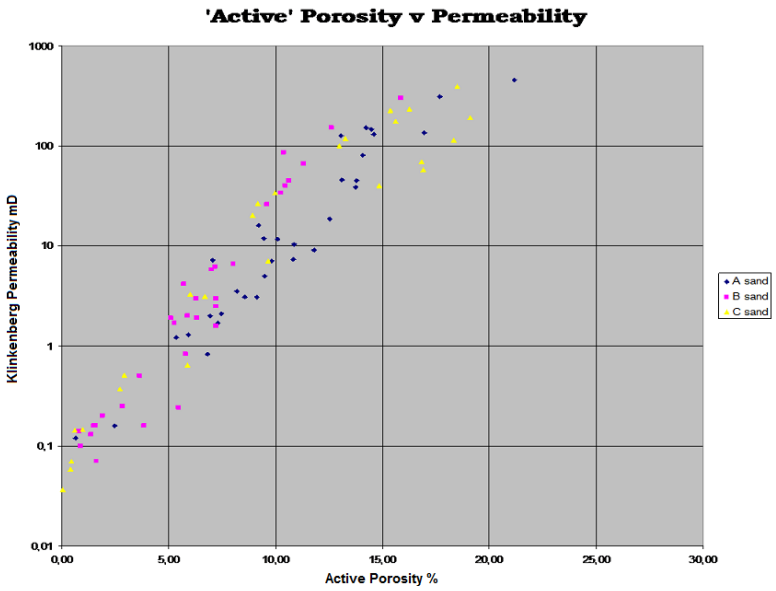

Figure 4.7: Permeability plotted against active porosity for the three reservoir units. Permeability in mD on logarithmic scale, porosity in %. Same trend as Figure 4.6, less scatter[18].

4.6 S_{wirr} & P_D

Ian Reid argue that once the permeability is known, the irreducible water saturation, S_{wirr}, and the displacement pressure, P_D can be calculated through empirical relations. These relations are found through an extensive evaluation of the complete core material for the whole field. The relations are presented in Table 4.1.

Unit	$\mathbf{S}_{wirr}$	$\mathbf{P}_D$
A and C	$70.124 \cdot k^{-0.1483}$	$11.119 \cdot k^{-0.3154}$
B	$54.441 \cdot k^{-0.1857}$	$8.2487 \cdot k^{-0.3334}$

Table 4.1: Table showing the relation between permeability and irreducible water saturation and displacement pressure. The permeability used should be k_{res}[18].

Note that k_{res} should be used in the formulas presented in Table 4.1 To use these formulas the implicit assumption that capillary pressure translates from ambient to reservoir conditions is taken. There is also need to set

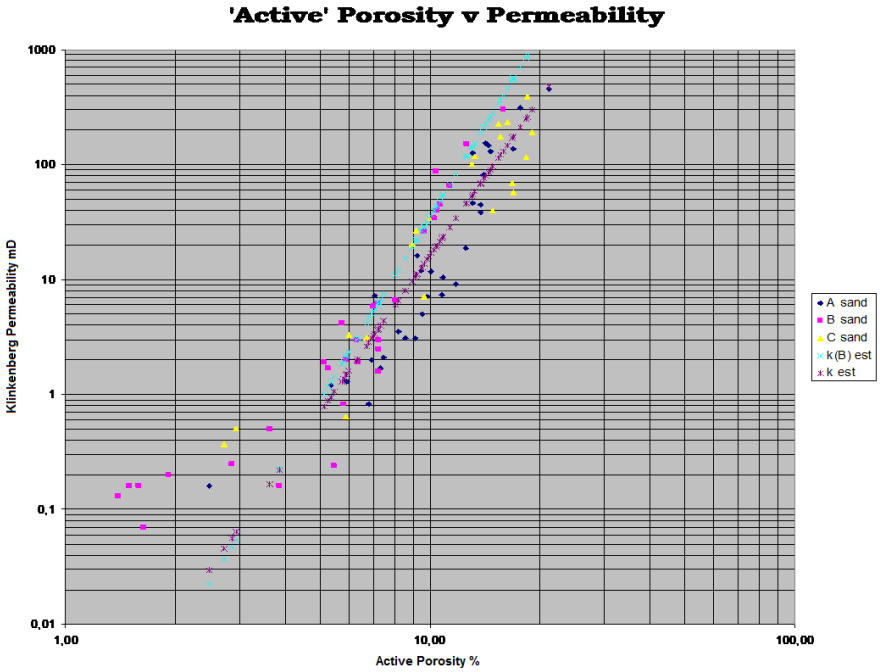

Figure 4.8: Permeability plotted against active porosity for the three reservoir units. Permeability in mD on logarithmic scale, porosity in %. Trend line for units A and B together, separate for unit B[18].

pragmatic limits for k_{res} to k_{res} >0.1 mD[18].

4.7 Saturation height model

The new saturation-height model on Gyda is fairly complicated. The saturation-height model aims to calculate the water saturation at any height above the free water level(haFWL), as shown in Figure 3.10, also evident from this figure is S_w=f(P_c). Instead of using the more common Leveret J model, the Thomeer model is used. The reasons for this choice are that the Leveret J function assumes an explicit relationship between porosity and permeability, which is not apparent for Gyda. Further, a log-log plot og capillary pressure vs Leveret J saturation should give a linear relationship, while the Thomeer gives a hyperbolic relationship. The data at Gyda gives a hyperbolic relationship as shown in Figure 4.9[18, 21].

Gyda is an old field, where several operators and service companies has been involved, resulting in differing data acquisition. P_c and S_w are taken

from core experiments, where the P_c is measured in an air-brine or air-mercury system, dependent on the core lab, and at ambient conditions. To make a capillary pressure curve for reservoir conditions, capillary pressure in an oil-brine system and reservoir temperature and pressure must be used.

In capillary tubes P_c is given as

$$P_c = \Delta\rho g h, \tag{4.12}$$

where $\Delta\rho$ is the density difference between the two fluids involved, g is the gravitational constant and h is the haFWL. $\Delta\rho$ and g can be combined together forming the gradient for the two fluids, rather than the density difference. Further the air-brine/mercury to oil-brine and ambient T and P to reservoir T and P has to be taken into consideration. Combining the gradient with the corrections mentioned an correction factor, C, can be introduced, rendering equation (4.12)

$$P_c = C \cdot haFWL. \tag{4.13}$$

The C contain among other the conversion of the capillary pressure from the formula

$$P_{cOB} = \frac{(\sigma cos(\theta))_{OB}}{(\sigma cos(\theta))_{AX}} \cdot P_{cAX}, \tag{4.14}$$

where OB denotes oil-brine system parameters and AX denotes air - brine/mercury parameters. The values of C is hard to determine as a range of possible values for interfacial tension and contact angle for combinations of fluids has been published. Furthermore there are uncertainty in the true densities of oil and water at reservoir conditions. The model comes up with a range for the C, being 0.8 to 2.0 with a mean of 1.5. This means that we can now utilise equation(4.13) for a range of haFWL to find the capillary pressure curve for a given well.

P_c is now, along with permeability and rock type, the input for determining the water saturation above the free water level. Permeability is taken from logs, empirical correlated to porosity. The rock type is expressed through a geometrical shape factor, G, which is defined for each unit of reservoir, values presented in Table 4.2. The derivation of the G-factor will not be shown in this thesis, however G=f($P_c^{\#}$, $S_w^{\#}$) where $P_c^{\#}$ and $S_w^{\#}$ is defined below.

Once G is known the theory for determining the water saturation, S_{wcap}, is given by the following equations

$$P_c^{\#} = \frac{P_c}{P_D}, \tag{4.15}$$

Unit	A	B	C
-G	0.11	0.14	0.11

Table 4.2: Table showing the values of the geometrical shape factor, G, for the reservoir units. Note that negative G is given[18].

$$S_w^{\#} = e^{\left(\frac{-G}{log(P_c^{\#})}\right)}, \tag{4.16}$$

$$S_w^{\#} = \frac{1 - S_{wcap}}{1 - S_{wirr}}. \tag{4.17}$$

Validity for equation (4.17) is ensured if $P_c > P_D$, otherwise $S_{wcap}=1$. Both P_D in equation (4.15) and S_{wirr} in equation (4.17) are input from the logs through permeability. If the three above equations are used in the present order, with a C from the said range and appropriate heights, the water saturations can be found at any haFWL[22].

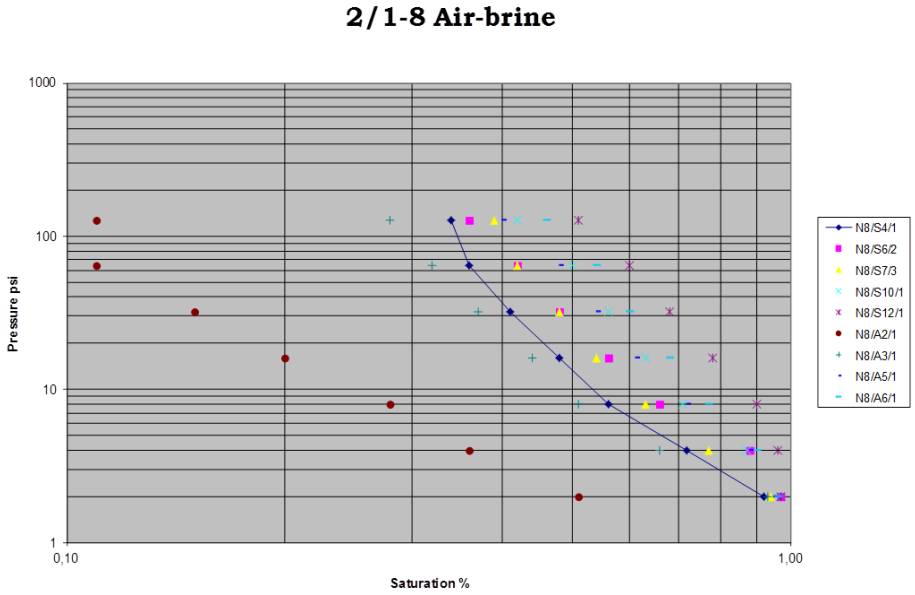

Figure 4.9: Capillary pressure plotted against water saturation for 2/1-8 well. Displays hyperbolic trend, meaning Thomeer model is most descriptive[18].

Chapter 5

Method

5.1 The Wells

The three well analysed in this report are as mentioned 2/1-A-12, 2/1-A-32 and 2/1-A-32. The three well spans across different reservoir zones as presented in section 2.2, the reservoir zones of each well is presented in Table 5.1 along with the zone tops. From the table it is evident that well A-12 spans reservoir zones 1 - 3, thus lies within the C-unit. A-30 and A-32 contains reservoir zones 1 - 4, where zones 1 - 3 are in the C-unit and zone 4 lies in the B-unit.

The wells exhibited different logging coverage and two out of the three wells there are core data available. Table 5.2 displays the log coverage for each well as well as core coverage.

Once the reservoir zones are established the calculations can be done on basis of Ian Reid's model. For the porosity calculations, the formula shown in section 4.1 should be used with values for matrix and fluid density shown in Table 5.3 for the respective zones.

In wells where the density log is absent in the reservoir intervals, sonic density should be used. Here a matrix transit time, Δt_{ma}, of 55 $^{\mu s}/_{ft}$ and a fluid transit time, Δt_f, of 200 $^{\mu s}/_{ft}$[17, 20]. In the calculation of clay fraction the values used in the double clay indicator, presented in section 4.2, is presented in Table 5.4.

The temperature gradient was set to 3.7 $^{\circ C}/_{100m}$[18] with reference depth and temperature of 4065 mTVDSS and 156°C respectively. For the saturation height calculations an C of 1.5 was used in equation (4.13). Figure 5.1 shows a set of cleaned up RFT data for the whole Gyda Field, excluding the Gyda South. Free water level was set at 4180 mTVDSS, after Figure 5.1[18].

MD	TVDSS	TOPS	Well identifier
5808.00	4053.93	BCU	2/1-A-12
5911.46	4122.63	Res Z_1	2/1-A-12
5922.86	4129.87	Res Z_2	2/1-A-12
5969.91	4159.16	Res Z_3	2/1-A-12
5521.00	4066.70	BCU	2/1-A-30
5565.41	4093.34	Gyda_top_strat	2/1-A-30
5605.26	4117.36	Res Z_1	2/1-A-30
5605.26	4116.31	Res Z_2	2/1-A-30
5634.02	4132.59	Res Z_3	2/1-A-30
5664.67	4149.94	Res Z_4	2/1-A-30
5548.23	4054.18	BCU	2/1-A-32
5620.88	4089.40	GYDA_top_strat	2/1-A-32
5733.96	4135.69	Res Z_1	2/1-A-32
5761.97	4146.56	Res Z_2	2/1-A-32
5824.21	4170.73	Res Z_3	2/1-A-32
5856.88	4183.41	Res Z_4	2/1-A-32

Table 5.1: Overview of reservoir zones present in each well and zone tops[23].

5.2 Log Analysis

The log analysis was done in accordance with the petrophysical model of Ian Reid[18], presented in chapter 4. Below follows a stepwise description of the log analysis for each well.

2/1-A-30

The A-30 well holds the most comprehensive log coverage as well as core data, so this well was analysed first. The well was split into zones in accordance with Table 5.1, A-30 holds no zone 1. Clay volume was determined as described in section 4.2 and Table 5.4. Intervals where neutron and/or den-

2/1-A-12	**2/1-A-30**	**2/1-A-32**
Gamma Ray	Gamma Ray	Gamma Ray
Sonic	Sonic	Sonic
Resistivity Shallow	Density	Density
Resistivity Medium	Density Correction	Density Correction
Resistivity Deep	Neutron Log	Resistivity Medium
Bit size	Resistivity Medium	Resistivity Deep
Cored	Resistivity Deep	Bit Size
	Bit size	Photoelectric Effect
	Photoelectric Effect	Caliper
	Caliper	
	Cored	

Table 5.2: List of logs present in each well, including if the well has core data.

sity log were absent, gamma ray log was used to determine clay volume with equation 4.4. GR_{min} and GR_{max} was determined by matching the two clay fraction curves in intervals where both methods was present. The resulting clay volume reveals that the reservoir zones can be considered as clean sand with only minute clay volumes, rendering Archie's law valid.

Total porosity was determined using density log and equation 4.1 with the appropriate values from Table 5.3. Furthermore active porosity was calculated using equation (4.7) and (4.8) setting cut off values for total porosity to 12.2 % and 5.3 % for C and B unit respectively. Seeing that the active porosity now calculated was under reservoir conditions it was transformed to

Parameter	**Zone 1**	**Zone 2**	**Zone 3**	**Zone 4**
Matrix density	2.654	2.654	2.659	2.652
Fluid density OBM	0.589	0.589	0.859	0.936

Table 5.3: Table displaying the parameters to be used in calculating the density from the neutron log for each reservoir zone. All densities in $^{g}/_{cc}$[17].

Parameter	**Zone 1**	**Zone 2**	**Zone 3**	**Zone 4**
Matrix density	2.654	2.654	2.659	2.652
Wet shale density	2.61	2.61	2.61	2.61
Fluid density OBM	0.95	0.95	0.95	0.95
Matrix neutron porosity	-0.03	-0.03	-0.03	-0.03
Shale neutron porosity	0.29	0.29	0.29	0.29
Fluid neutron porosity	1	1	1	1

Table 5.4: Table showing values used for each reservoir zone in the calculation of clay fraction. All densities in unit $^{g}/_{cc}$ and all neutron porosities in neutron porosity units[17].

ambient conditions using the relation in equation (4.3).

The ambient active porosity was used to calculate the permeability at ambient conditions using equation (4.9) and (4.10). To transform this permeability back to reservoir conditions equation (4.11) was used. Further irreducible water saturation and displacement pressure was calculated after equations shown in Table 4.1. The saturation height model was utilised with correction factor, C, set to 1.5 and Free Water Level set to 4180 mTVDSS, to find the water saturation from capillary pressure. The procedure described in section 4.6 was followed.

The permeability obtained matched poorly with the core permeability, exhibiting wide scatter with no systematic error, further, the saturation found from the capillary pressure model matched poorly with the Archie saturation. The mismatch appeared in the C-unit section of the well. A second log analysis was performed where Zone 3 was interpreted as a member of B-unit. Still showing poor correlation between cores and logs in Zone 2, the whole well was reinterpreted using only parameters for the B-unit. This lead to bad correspondence between the density and core density in the well above 5640 mMD. A new zone was split, called "unit B" along with the initial zone, "Unit B2". The densities were tuned to fit the core data. The densities used to get this fit was ρ_{ma}= 2.5 and ρ_{fl}= 0.8. Permeabilities, irreducible water saturation, displacement pressure, Archie saturation and capillary height saturation was then calculated as before.

2/1-A-12

The A-12 well also holds core data, but a poorer log coverage overall. In absence of neutron log, gamma ray was used to determine clay volume. GR_{min} and GR_{max} was chosen such that the clay volume in the reservoir zones would match those in well A-30. This is a valid assumption seeing that the wells are located in close vicinity. The clay volume is still minor, a zone small interval holding a fraction of 0.15 in reservoir zone 2 is the sole clay of importance.

Total porosity was calculated with the sonic log, as density log was absent. Equation (4.2) with the values stated above gave a fine correlation with the core porosity in zone 1 to a lesser extent in Zone 2. On basis of the total porosity, active porosity was determined using 12.2 % as cut off for the total porosity. Permeability was calculated with a good correlation in upper Zone 2. Downward Zone 2 the log permeability was somewhat off from the cores. Archie saturation and saturation from saturation-height model was calculated. S_{wcap} displays fine correlation with the core saturation but matched the Archie saturation poorly. To try to obtain the increasing saturation downwards, indicated by Archie, the FWL was set to 4140 mTVDSS, and S_{wcap} was calculated again.

On this well, a sensitivity analysis was carried out regarding the correction factor, C, and the choice of Free Water Level. Both parameters in the saturation height model, to check if the core saturations could be matched. The base case with a C factor of 1.5 and FWL set to 4180. The sensitivity analysis consisted of changing the FWL and keeping the C factor constant. Free Water Level was changed, keeping the C factor constant, giving the two additional heights of 4170 and 4190 mTVDSS. Whilst the C factor was changed to the limit values in the interval stated in section 4.6, 0.8 - 2.0, keeping the Free Water Level at 4180 mTVDSS.

As an attempt to better the correlation between poroperm logs and cores in mid Zone 2, an additional zone was made to change the fluid transit time. Getting a better correlation between the porosity log and cores, implicitly bettering the correlation for permeability as well. Δt_{fl} was set to 185, a fresh water value, to obtain better correlation.

2/1-A-32

The A-32 do have a neutron log, but this log is not recorded in the reservoir zones. Here as well as the A-12 well, gamma ray was used to determine the clay volume. Once again there are reason to assume similarity, and equal

clay fraction, between the wells. A mean clay fraction on 0.03 in the reservoir sections is the highest of the three wells, but still not significant.

As stated earlier, the A-32 well contained reservoir Zone 4, the logs are however not taken in this zone, leaving this zone uninterpreted. Density log was used to calculate the total porosity. Input in the density formula after Table 5.3. Permeability was found, using 12.2 % as cut off for the total porosity, through equation (4.7). Archie saturation, irreducible saturation and saturation height model was found analogues to the prior wells.

CPI-plot was made on all wells, along with plots of the alternative interpretations and sensitivity analysis. Comparative plots where made between the interpretation from the new model versus the old interpretations. Porosity, permeability and water saturation was plotted in the same tracks, making it easy to spot differences.

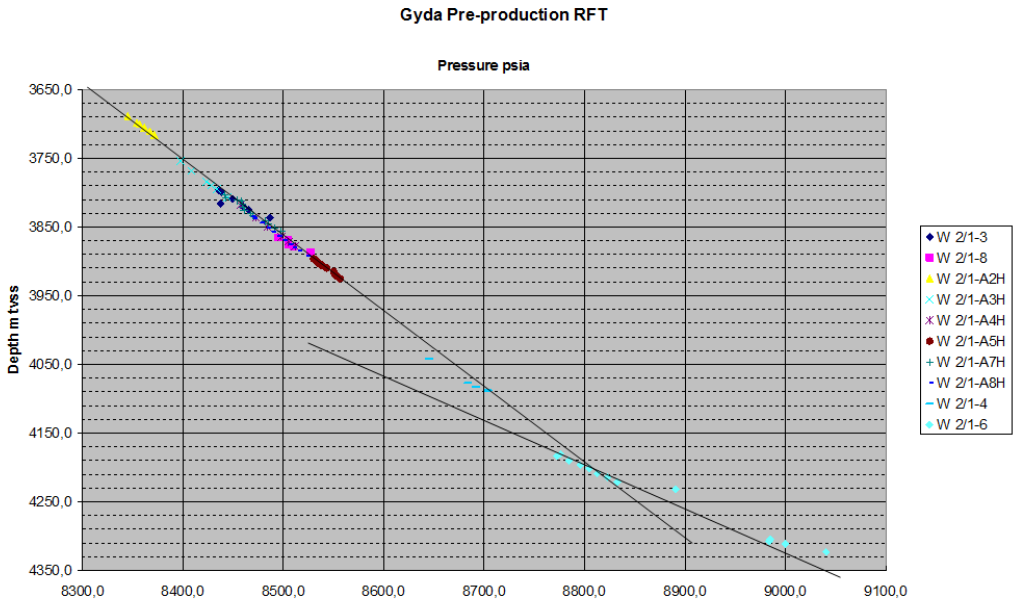

Figure 5.1: RFT data for whole Gyda Field. Showing FWL to be at 4180 mTVDSS[18].

Chapter 6

Log Assessment

All log plots presented in the Appendix.

6.0.1 Well A-12

CPI-plot

Figure A.1 is the CPI for well A-12 made after the new model of Ian Reid. Gamma ray is constant, indicating sand without significant pollution, reflected in the V_{cl} plotted in the volumetric track. The resistivity logs exhibits very low resistivity. The clean sand containing rather salty water can cause this low resistivity. The spike in resistivity at approximately 5943 mMD indicates a low permeability zone.

Looking at the porosity track the total porosity matches the core porosities in Zone 1 and top Zone 2, the cores lower down indicates that the model underestimates the porosity here. The active porosity is cut off at 12.2 % of ϕ_{tot} and thus the zones having a ϕ_a of zero is defined as non net sand. The implications of this is evident for the model permeability, seeing that it is a function of porosity and permeability thus is zero when the active porosity is zero. The core permeabilities matches good in the same upper part of Zone 2 as the porosities did.

The saturations obtained through the saturation height model, curve Sw_cap-_mod in track 10, seems somewhat chaotic in Zone 1 and lower half of Zone 2. The fluctuating spikes arise from the formulas which the saturation is calculated from, and the fact that they depend on the capillary pressure. This is also given from the model through the correction factor ,C. In the upper half of Zone 2 the saturation matches the core saturation sufficiently. The Archie saturation, curve SwArch_mod, is systematically higher than the cores. Core saturation has a rather bad reputation within the industry, es-

pecially on older wells. At best, core saturations can be used as a trend indicator, not taking the values as hard facts. What is clear is that the Archie saturation indicates a contact somewhere below 5936 mMD, this is supported by the drop in resistivity. Local variations in the OWC can occur, as faults at these depths often are tight, hindering communication in the reservoir. The model saturation does not support this, as it indicates low saturations across the whole bottom interval. The misrepresentation here is again caused by the way the saturation is calculated. The saturation is correlated with permeability through P_D, S_{swirr}. The only limiting factor is the capillary pressure which is calculated on basis of a chosen Free Water Level. The field-wide FWL of 4180 mTVDSS is here to deep, causing the water saturation to drop below what is indicated as a contact. An attempt of dismissing these saturation values in the lower interval is done through a sensitivity study shown in Figure A.3 and will be reviewed below.

The volumetric track shows room for hydrocarbons at 5923 - 5936 mMD, with the contact located somewhere below.

Porosity fitting

In Figure A.2 the mismatch between model porosity and core porosity was removed by tuning the parameters for fluid transit time in the current interval. The resulting match was an improvement both regarding porosity and permeability, which still did not match fully. This alternation of the porosity had a heavy influence on the saturation, pulling the Archie saturation down and the saturation from the saturation height model up. The Archie saturation does approach 1 for the lower section, but not in the same manner as the on the original CPI, leaving it hard to determine the contact, if one.

Sensitivity analysis

Track 4 and 5 in Figure A.3 shows the sensitivity analysis done for the saturation height model. Here Free Water Level has been held constant whilst the C-factor has been altered (Track 4), and C-factor altered whilst Free Water Level was changed (Track 5). In both tracks it is evident that the difference between the curves increases downwards to the Free Water Level. The other apparent, and somewhat anti intuitive, result is that in either track the base case is the one giving the lowest saturation. Track 6 shows the model saturation with FWL set at 4140, 4145 and 4150 mTVDSS. This was done to try to obtain the Archie saturation. The apparent problem being that the model does not give an output below the chosen FWL. Also the fluctuations are very much present.

Comparison

I the comparison plots the porosity, permeability and water saturation from the new model and the old model are plotted in the same track to show the difference clearly. Shading has been applied in Track 3 and 4, where yellow shading indicates interval where the new values are higher and red shading where the old model gives higher values.

The porosity is quite similar, but the permeability is not. The new model predicts a permeability consistently lower than the old. This indicates a different correlation between porosity for the two models. Knowing the good correlation between core and log permeability from the new model this one might lead to accuse the old model of overestimating the permeability. The water saturation is also quite similar. Showing very good coincidence in top Zone 2. Both saturations closes into 1 downward Zone 2.

6.0.2 Well A-30

CPI-plot

The CPI-plot for well A-30 is shown in Figure B.1 and the plot reveals that this also is a clean sand. Further the neutron density track shows good negative separation indicating hydrocarbons. The large separation in upper half of Zone 2 can indicate gas, before the separation decrease indicating oil. The neutron log abruptly ends at 5650 mMD, the most probable cause is tool failure. The well report, however, does not mention this especially. The water oil contact does not appear in the interval plotted.

The porosity estimation seems to be somewhat over estimating the cores, and the active porosity cut-off of 12.2 % yields a low net sand fraction in Zone 3 in particular. This further influences permeability which correlates to a minor extent in Zone 2. The model permeability in Zone 3 does not fit at all, predicting the cored interval as tight, while the cores averages on about 1 mD. The saturation calculated shows a good fit with the Archie saturation in Zone 4, a little over estimation in Zone 2, but completely off in Zone 3. This due to the already mentioned dependency on the permeability.

Reinterpretation

The original model plot failed profoundly to represent permeability and water saturation in Zone 3, thus this zone was reinterpreted as a B-unit member. The result is shown in Figure B.2 where the porosity, permeability and saturation are plotted over again. The largest effect of assigning B-unit properties to Zone 3 was the active porosity cut off, seeing that it is as low as 5.3 %

of total porosity. Along with the different correlations, this gave a far larger net sand interval, along with boosting the permeability in the zone previous deemed as tight. The model saturation from the saturation-height is still somewhat high, but much better than in Figure B.1.

To try to get a better match for the saturations, especially in Zone 2, the whole interval was reinterpreted as B-unit member with two zones, see Figure B.3. This caused the model saturation to under predict the saturation compared to the Archie saturation. The core permeability in Zone Unit B does still not match the cores, reason being that the porosity still is somewhat high.

Comparison

Figure B.4 shows the comparison between the old and the new model. The porosity is quite similar, the old model tend to lie above. The same trend is apparent for permeability, the old permeability curve is in general larger than the new curve. The obvious difference being that the old model do not predict any permeability in Zone 4 at all, while the new model gives the zone good properties. The two saturation curves matches good.

6.0.3 Well A-32

CPI-plot

The CPI-plot for well A-32 is shown in Figure C.1. There are no cores for this well, but the was used as an reference well when the model was made so a good representation should be expected. The plot does reveals good correlation between the Archie and the saturation-height saturation. Down in Zone 3, where a water oil contact is expected the same problem arises, as for well A-12. The Archie saturation approaches 1, while the model saturation fluctuates a lot more, not revealing the same trend towards 100 % water saturated. This is, yet again, linked to the chosen Free Water Level, which is set to 4180 mTVDSS.

The comparison plot in Figure C.2 exhibits a good match. The porosity obtained from the new model does overlie in Zone 1 and 2, with the other way around in Zone 3. The permeability track shows that the old model estimates the permeability higher across the whole reservoir, but only minor differences. The saturation curves stacks down to 5830 mMD, where the old fluctuates around 0.95 water saturation and the new goes to 1 at 5835 mMD.

Chapter 7

Conclusion

The new petrophysical model on Gyda has been tested on three wells. The model uses standard method for total porosity calculation. The active porosity defining net sand and subsequently the permeability seems to yield a good description of the well. The crucial factor regarding the net sand and active porosity determination is the zonation, the zone must be assigned to the correct reservoir unit. If this is not the case, the data given by the model would be a severely misrepresentation. On the other hand, this characteristic of the model can be used to determine reservoir zones by matching against cores, or look at the saturations for matching.

The saturation from capillary pressure and height above Free Water Level, the saturation height model, yields good match with the Archie saturation as long as the reservoir zone is assigned the right unit, and the Free Water Level is set to the correct height. The model also has a tendency to become unstable near the set Free Water Level.

The comparison with the old model shows that the two model gives similar values on both porosity, permeability, and water saturation, with equal differences either way. The full implications of the new model will be apparent once the whole field is evaluated and this is used on in simulations.

Appendix A

Well A-12

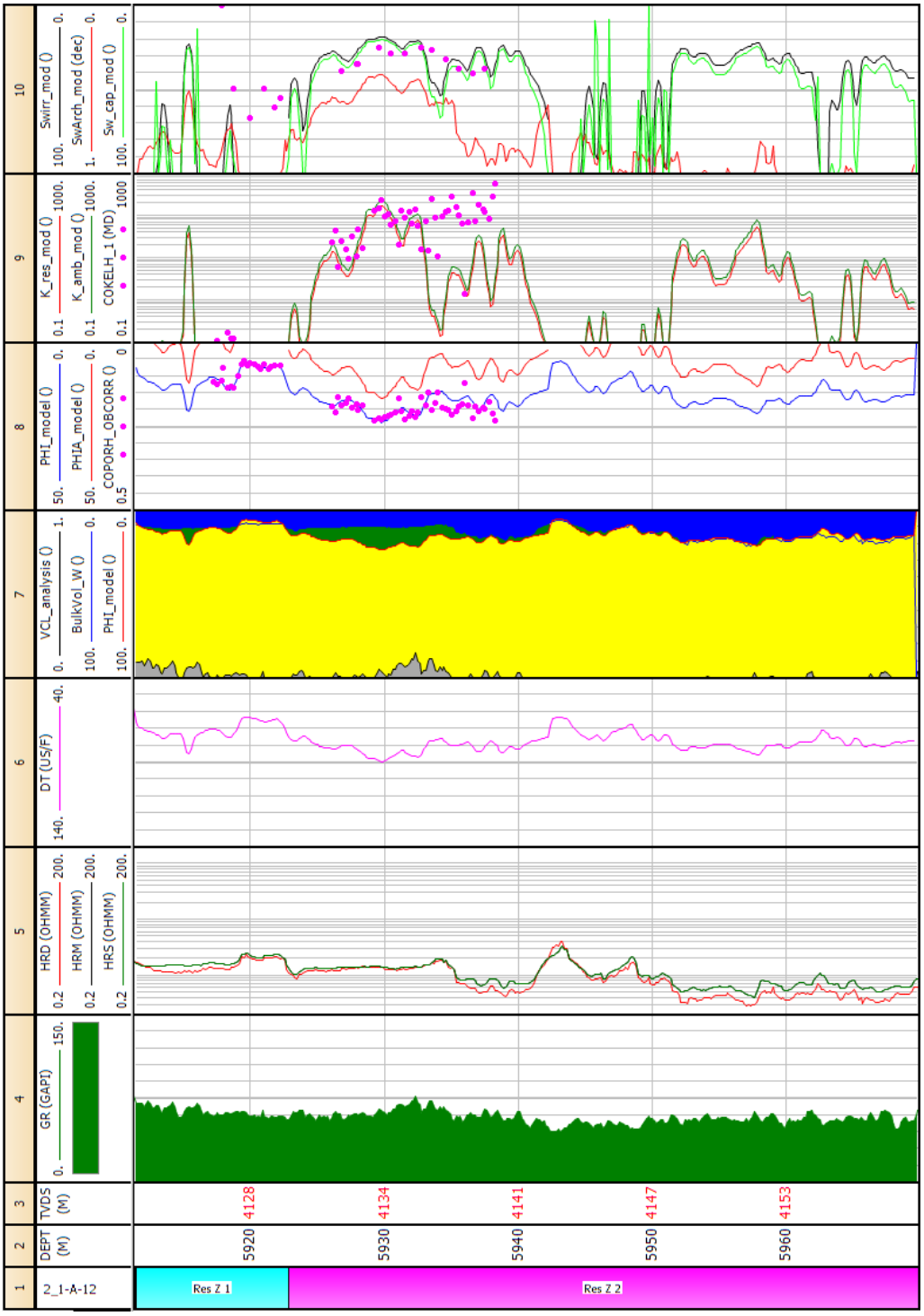

Figure A.1: CPI-plot for the A-12 well. Interpretation done in accordance with the new model.

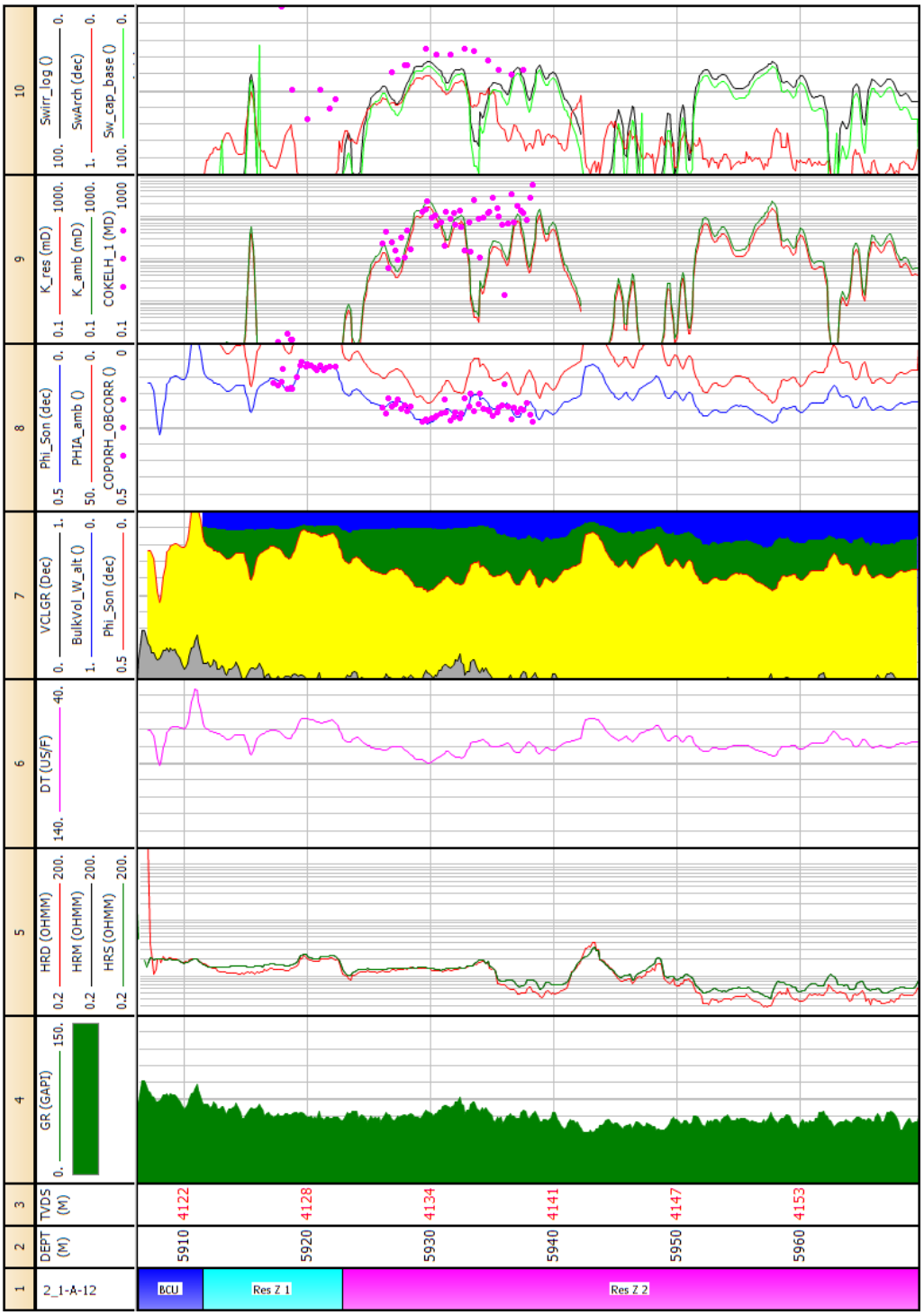

Figure A.2: CPI-plot for the A-12 well. Porosity curve tuned to fit core porosity.

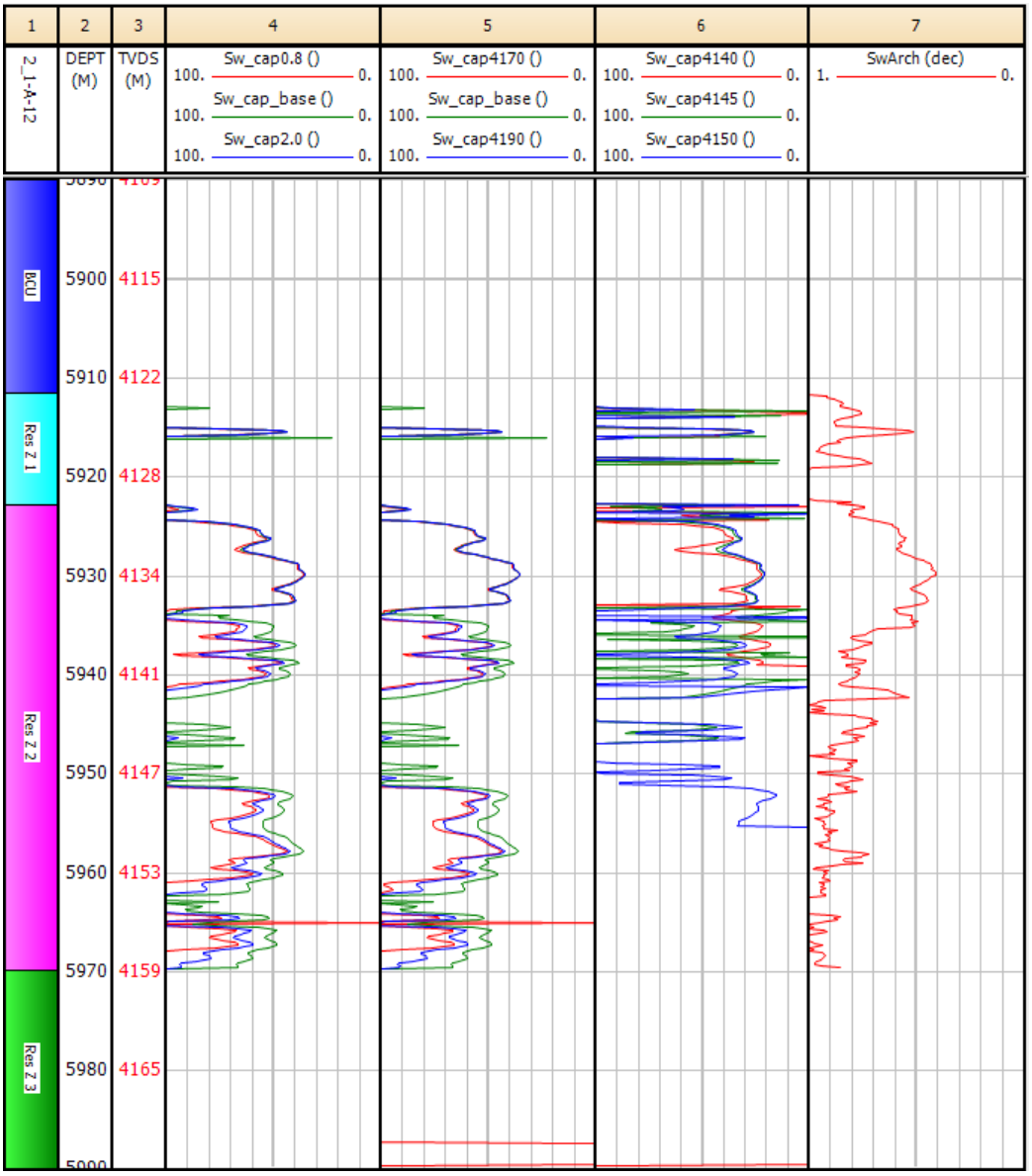

Figure A.3: Plot showing the sensitivity analysis for the saturation height model. Free Water Level and correction factor, C, changed.

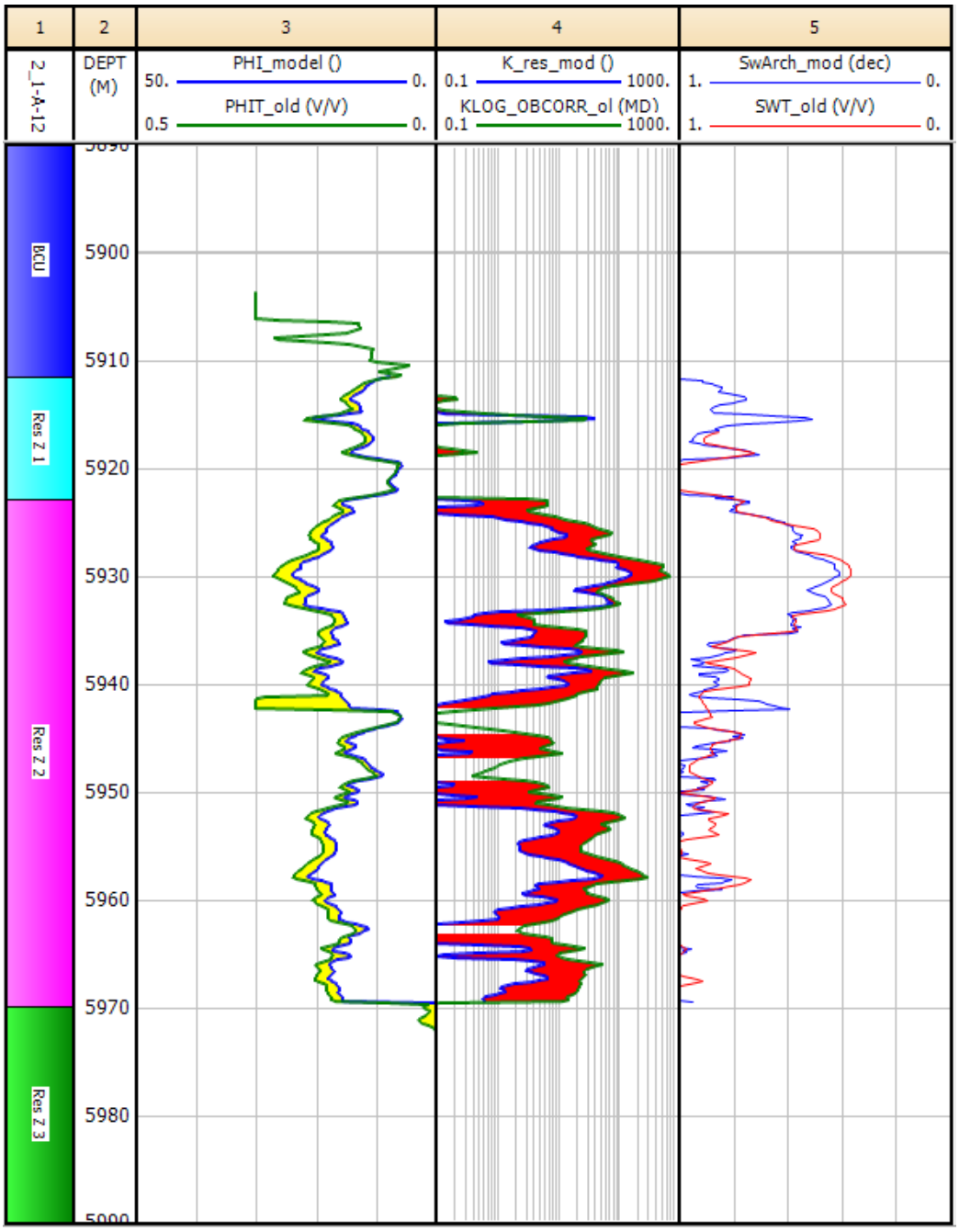

Figure A.4: Plot comparing porosity, permeability and water saturation between the new and old Gyda model.

Appendix B

Well A-30

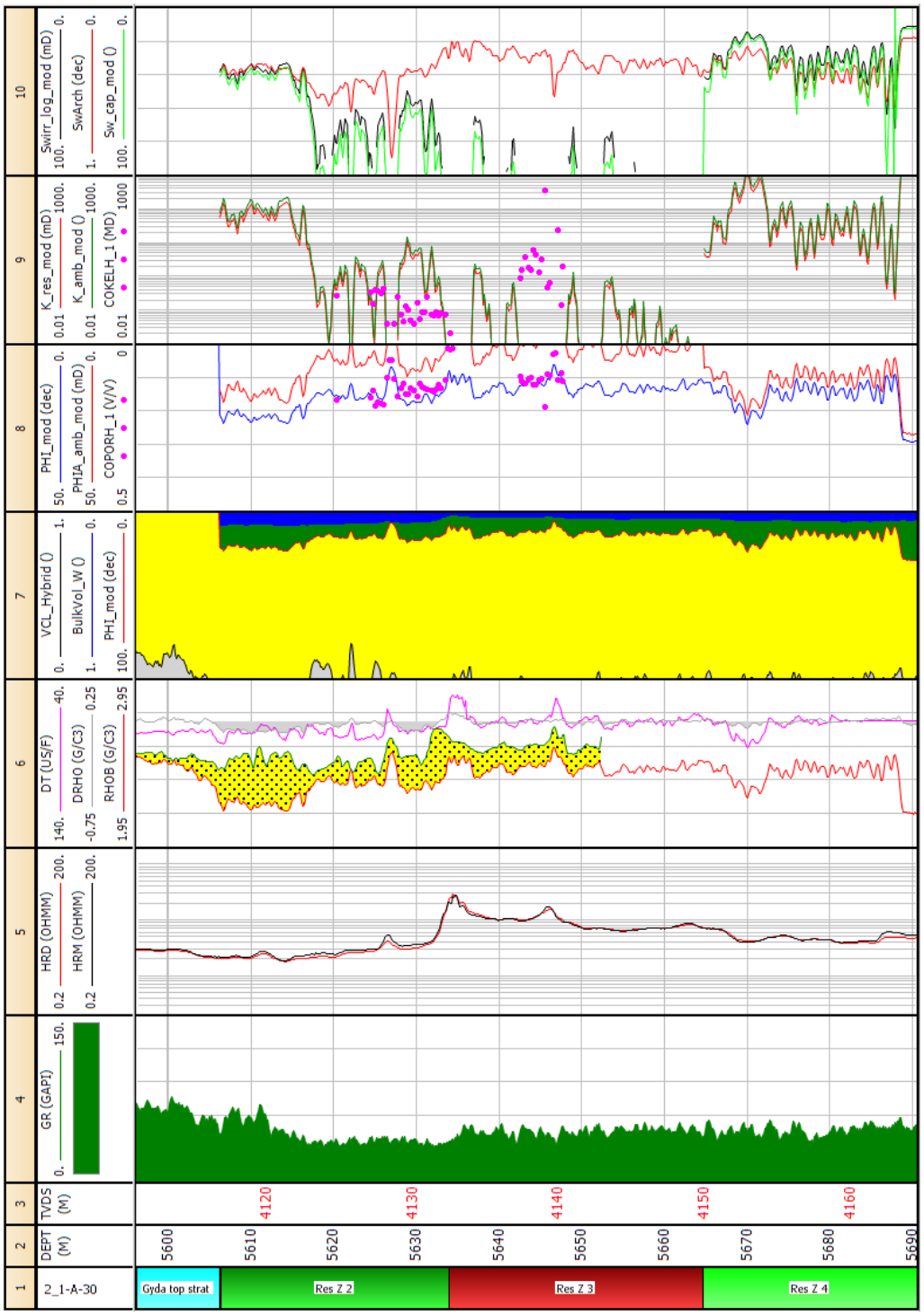

Figure B.1: CPI-plot for the A-30 well. Interpretation done in accordance with the new model.

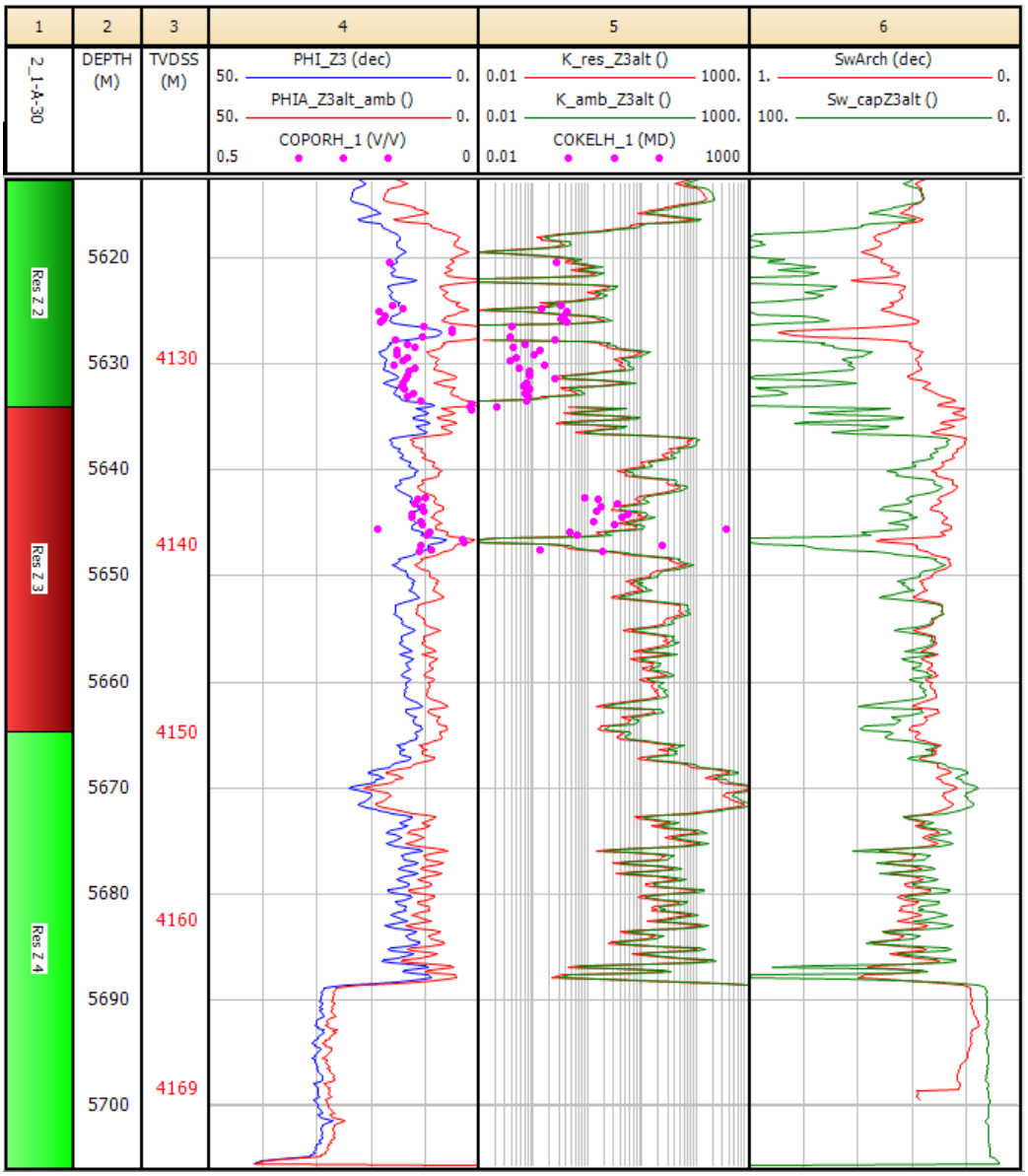

Figure B.2: Reinterpretation of A-30 well, Zone 3 interpreted as B-unit sand.

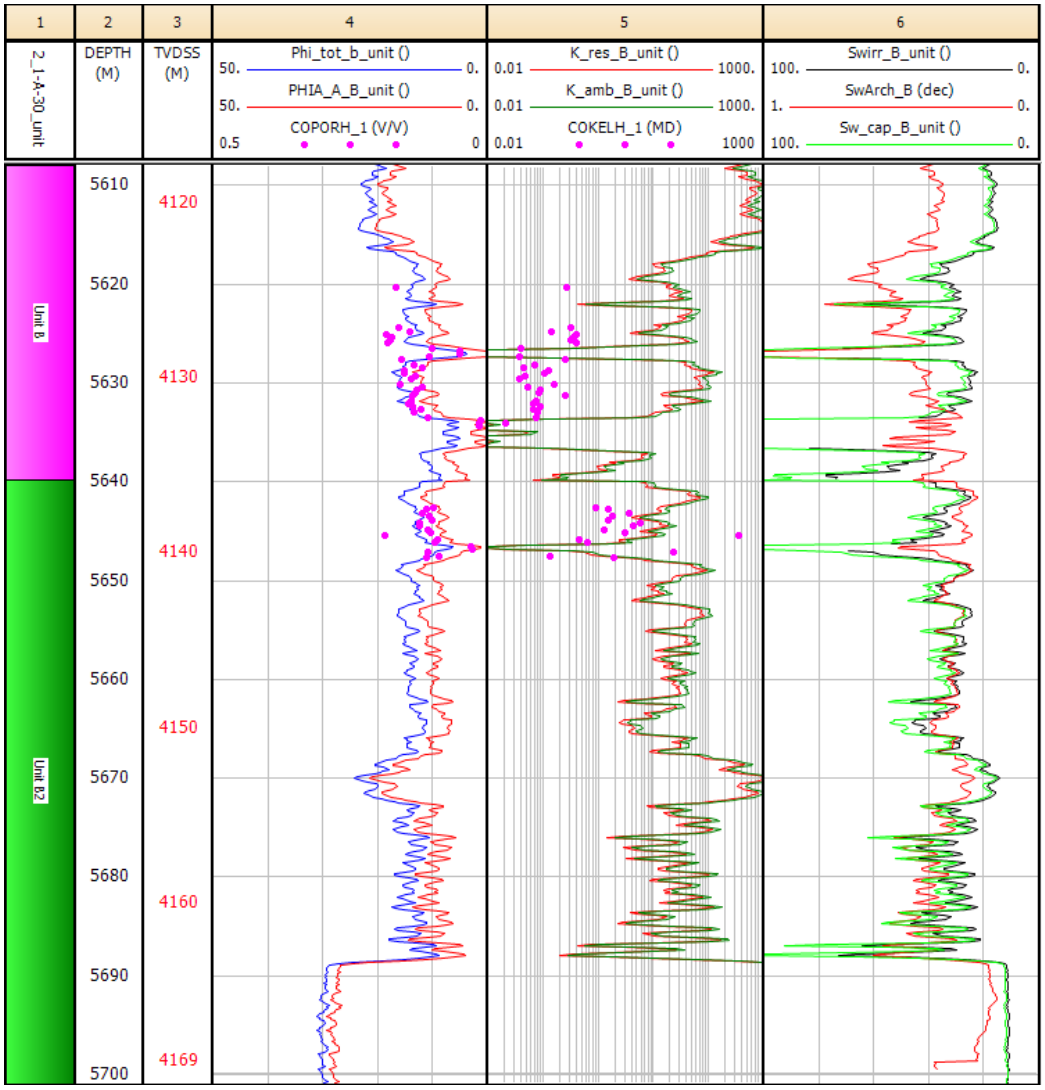

Figure B.3: Reinterpretation of A-32 utilising B-sand parameters across whole reservoir interval.

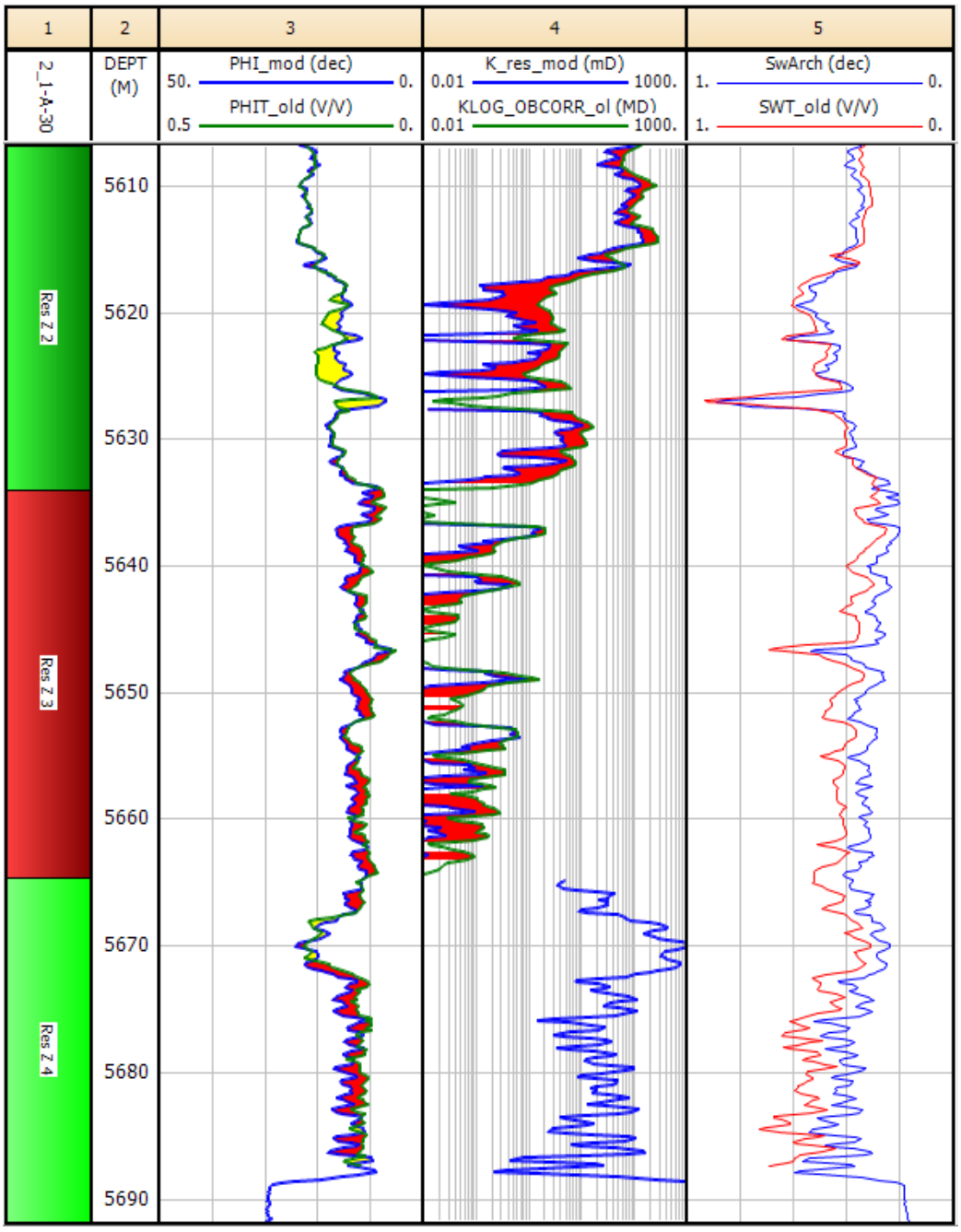

Figure B.4: Plot comparing porosity, permeability and water saturation between the new and old Gyda model.

Appendix C

Well A-32

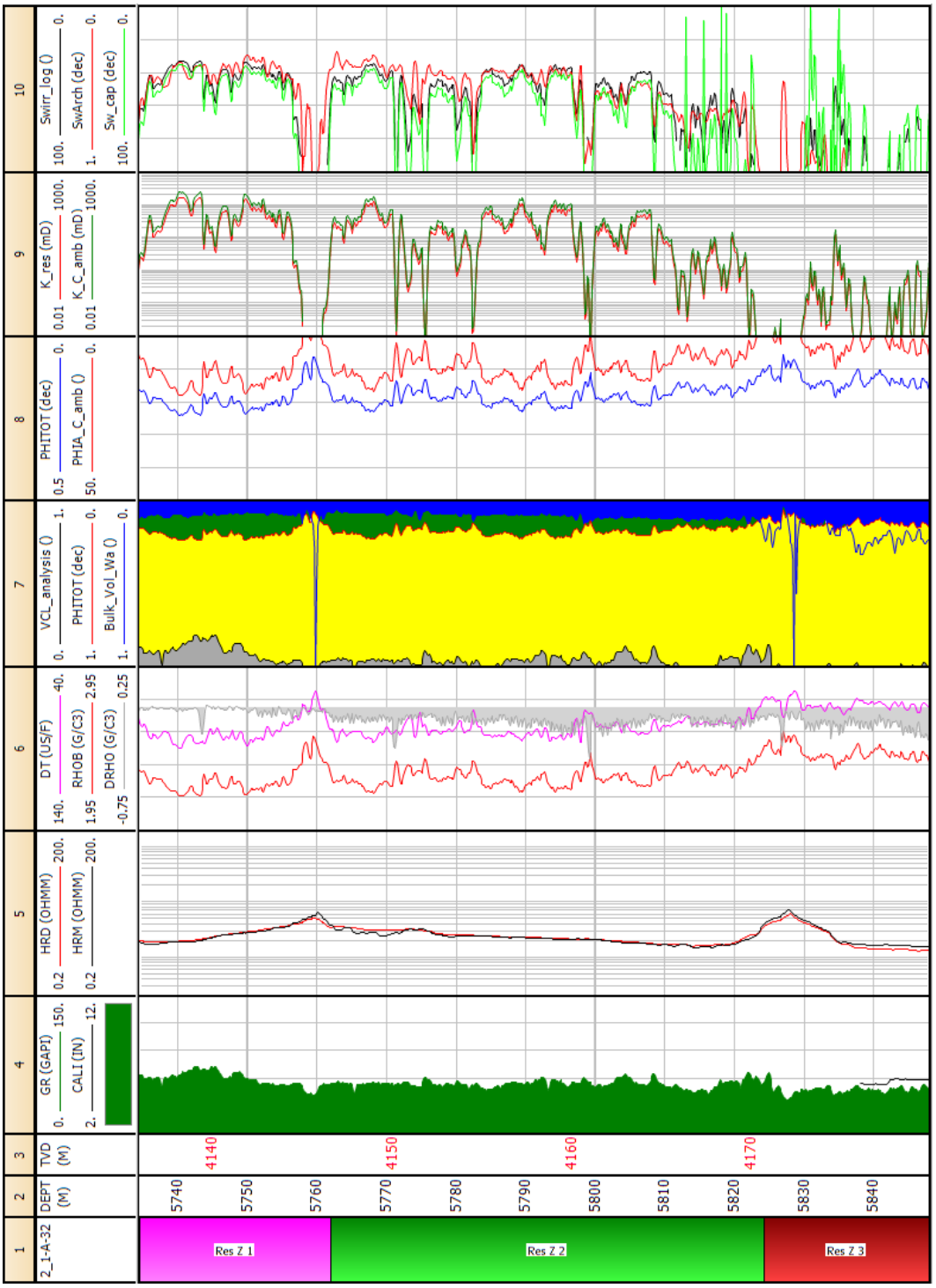

Figure C.1: CPI-plot for the A-32 well. Interpretation done in accordance with the new model.

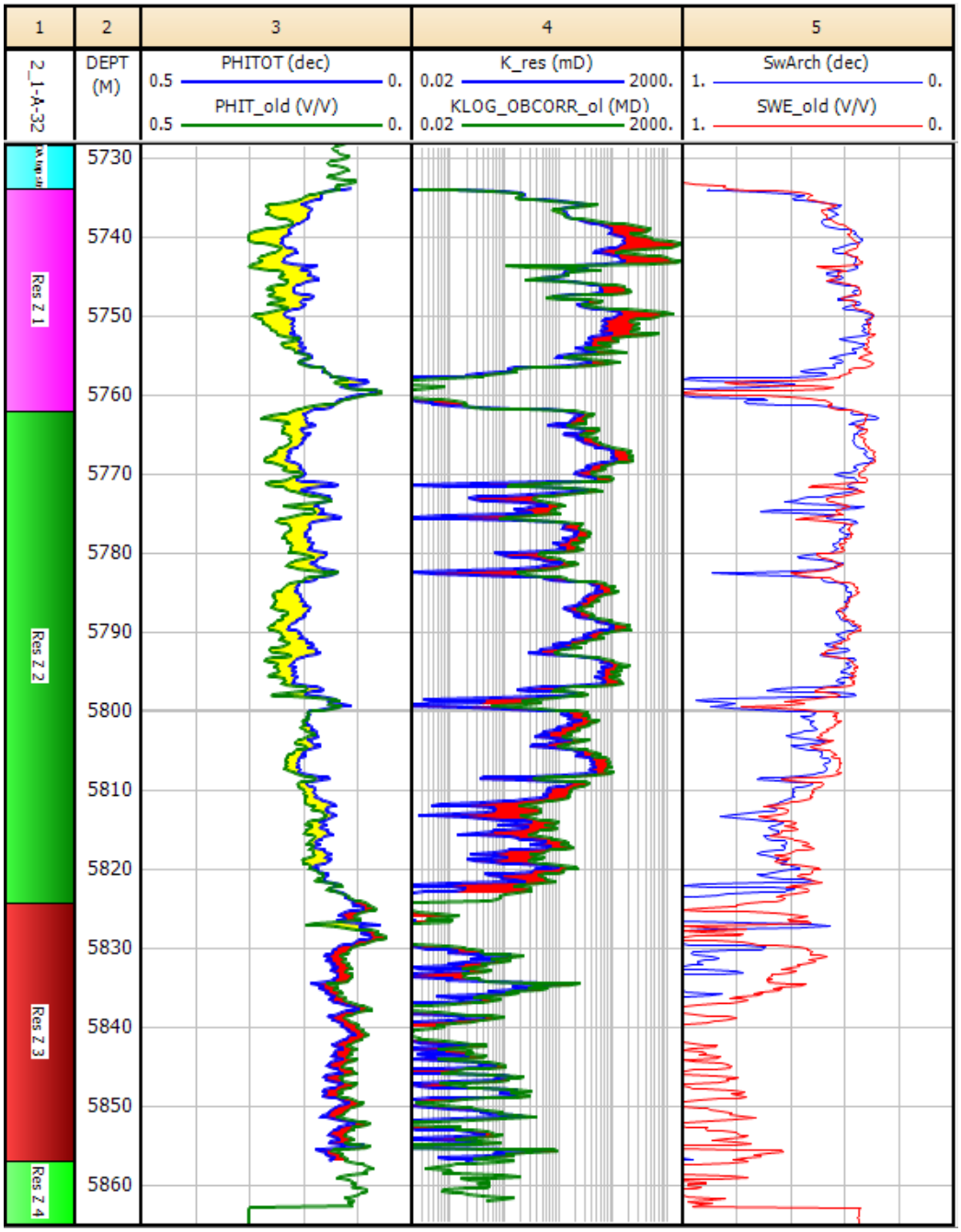

Figure C.2: Plot comparing porosity, permeability and water saturation between the new and old Gyda model.

Bibliography

[1] C & C Reservoirs. Field evaluation report, gyda field, February 2001. Revised February 2008.

[2] The Norwegian Petroleum Directorate. Field information on gyda. `http://www.npd.no/global/norsk/3-publikasjoner/faktahefter/fakta2011/figurar/kapittel-10/gyda.pdf`.

[3] The Norwegian Petroleum Directorate. Fact maps. `http://npdmap1.npd.no/website/npdgis/viewer.htm`.

[4] Talisman Energy Norge. Gyda introduction. Technical report, Power Point presentation made for internal use in Talisman, 2011.

[5] Norwegian Petroleum Museum. Ekofisk fact page. `http://www.kulturminne-ekofisk.no/`.

[6] BP Petroleum Norway Limited. Development and operations plan for the gyda field, 1987.

[7] The Norwegian Petroleum Directorate. Facts on ula formation. `http://www.npd.no/engelsk/cwi/pbl/en/su/all/179.htm`.

[8] Tarek Ahmed. *Reservoir Engineering Handbook*. Elsevier, 2010. Fourth edition.

[9] Zaki Bassiouni. *Theory, Measurement and Interpretation og Well Logs*. Society of Petroleum Engineers, 1994. SPE textbooks series Volume 4.

[10] Karl Audun Lehne. *Geologisk brønnlogging*. Universitetsforlaget, 2003.

[11] Malcom Rider. *The Geological Interpretation of Well Logs*. Rider French, second edition edition, 2008.

[12] Karl Audun Lenhe. Scal analysis. Powerpoint from course Formation Evaluation.

[13] J. R. Ursin and A. B. Zolotukhin. Compendium to reservoir engineering i course, 1997. University of Stavanger.

[14] The Discovery Group Inc. `http://www.discovery-group.com/pdfs/Archie%20Hingle%20Pickett.pdf`.

[15] HyperPhysics website. `http://hyperphysics.phy-astr.gsu.edu/hbase/surten.html`.

[16] Luca Cosentino. *Integrated Reservoir Studies*. Institut Francais du Petrole Publications, 2001.

[17] Jonathan Hall. *Gyda Petrophysical Review 2011*. DONG Energy.

[18] Ian Reid. Presentation of the gyda petrophysical model. Internal Talisman document, 2012.

[19] Ian Reid. Answer letter on questionnaire.

[20] BP Elxploration. *Gyda Field Petrophysical Study*. BP.

[21] Ian Reid. Conversation on e-mail.

[22] Ian Reid. Second answer letter on questionnaire.

[23] Internal Excel sheet in Talisman.